Czech Technical University in Prague

Faculty of Electrical Engineering
Department of Cybernetics and Robotics

The I2T5: Enhancement of the Thermal Design of an Iodine Cold Gas Thruster

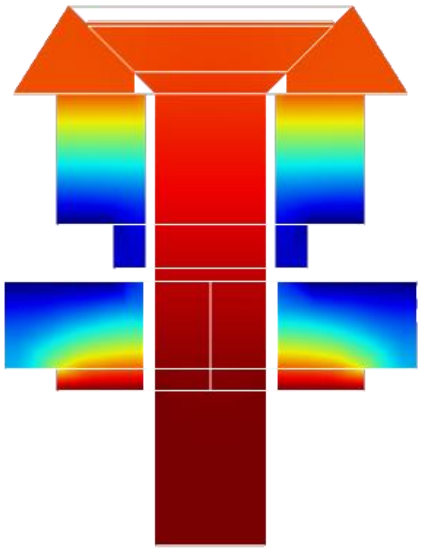

MASTER'S THESIS

Roger Michael Pereira

SpaceMaster Programme, 120 Credits

2020

The I2T5: Enhancement of the Thermal Design of an Iodine Cold Gas Thruster

Master's Thesis

Submitted in partial fulfilment of the requirements for the degree of

Joint European Master (SpaceMaster)

Awarded by

Czech Technical University in Prague	M.Sc. in Cybernetics and Robotics
Luleå University of Technology	M.Sc. in Space Science and Technology

Authored by

Roger Michael Pereira

Supervisor:	Javier Martínez Martínez	ThrustMe, France
Examiners:	Dr. Martin Hlinovský	CTU, Prague, Czech Republic
	Dr. Kristian Hengster-Movric	CTU, Prague, Czech Republic
	Dr. Anita Enmark	LTU, Kiruna, Sweden

August 14, 2020

ZADÁNÍ DIPLOMOVÉ PRÁCE

I. OSOBNÍ A STUDIJNÍ ÚDAJE

Příjmení: **Pereira** Jméno: **Roger** Osobní číslo: **489935**

Fakulta/ústav: **Fakulta elektrotechnická**

Zadávající katedra/ústav: **Katedra řídicí techniky**

Studijní program: **Kybernetika a robotika**

Studijní obor: **Kybernetika a robotika**

II. ÚDAJE K DIPLOMOVÉ PRÁCI

Název diplomové práce:

Zlepšení tepelné konstrukci za studena plynu Jód pohonného systému

Název diplomové práce anglicky:

Enhancement of the Thermal Design of a Cold Gas Iodine Thruster

Pokyny pro vypracování:

Seznam doporučené literatury:

[1] Rafalskyi, Dmytro, et al. "Thermal Validation Campaign of the Electric Propulsion System NPT30 Integrated Into the ISIS 8U Structure." (2019).
[2] Rafalskyi, Dmytro, and Ane Aanesland. "A neutralizer-free gridded ion thruster embedded into a 1U CubeSat module." International Electric Propulsion Conference. Vol. 10. 2017.
[3] Aanesland, Ane, et al. "The PEGASES gridded ion-ion thruster performance and predictions." IEEE Transactions on Plasma Science 43.1 (2014): 321-326.
[4] Talvistu, Siiri. "EM emissions test platform implementationfor satellite electric propulsion systems and electronic subsystems," Kiruna, Sweden (2019).

Jméno a pracoviště vedoucí(ho) diplomové práce:

Javier Martínez Martínez, katedra řídicí techniky FEL

Jméno a pracoviště druhé(ho) vedoucí(ho) nebo konzultanta(ky) diplomové práce:

Ing. Martin Hlinovský, Ph.D., katedra řídicí techniky FEL

Datum zadání diplomové práce: **14.02.2020** Termín odevzdání diplomové práce: **14.08.2020**

Platnost zadání diplomové práce:
do konce zimního semestru 2021/2022

Javier Martínez Martínez	prof. Ing. Michael Šebek, DrSc.	prof. Mgr. Petr Páta, Ph.D.
podpis vedoucí(ho) práce	podpis vedoucí(ho) ústavu/katedry	podpis děkana(ky)

III. PŘEVZETÍ ZADÁNÍ

Diplomant bere na vědomí, že je povinen vypracovat diplomovou práci samostatně, bez cizí pomoci, s výjimkou poskytnutých konzultací. Seznam použité literatury, jiných pramenů a jmen konzultantů je třeba uvést v diplomové práci.

. | Datum převzetí zadání

Podpis studenta

Abstract

The I2T5, an iodine-propelled, cold gas thruster, developed by ThrustMe, France, is the first of its kind to make it successfully to space. Due to its simple, reliable and cost-effective design, it is a suitable propulsion system for CubeSat missions with low delta-V (ΔV) requirements. To ensure that the I2T5 performs at its peak, it is crucial to maintain good thermal control of the thruster, to keep it within the operational temperature range.

The first flight measurements of the I2T5 provided insight into its thermal performance. It was observed that the required temperature to sublimate the iodine propellant was not reached within the expected time frame, which led to a longer warm-up period, and a reduction in thrust. The problem arose due to an unforeseen conductive thermal contact between the tank and the thruster walls.

This thesis delves deeper into this issue, and focuses on alleviating the total conductive heat loss from the tank to the satellite frame, where the I2T5 is integrated. The insulating washer-bolt configuration of the I2T5 side panels is observed to be responsible for the conductive heat transfer. A preliminary analysis is performed to obtain an initial maximum for the conductive heat flux lost to the satellite frame. A plan of action is then determined to optimise the geometry, material or configuration of the insulating washers to lower the maximum heat flux value. Following this, an experiment was conducted with a new washer-bolt configuration to determine the heat flux values. A case study is performed for the orbital environment heat fluxes that the I2T5 would receive if it were integrated to a CubeSat in sun-synchronous orbit.

An overview of results shows that, for the thermal simulations, all the methods employed to reduce the conductive heat loss at the frame were effective. The experiment provided neutral results, and would need to be repeated with different experimental parameters to have a clear perspective of the heat losses. In reality, the satellite frame receives radiative fluxes in addition to conductive heat fluxes, but radiation is not considered for this thesis, and is suggested as a prospective study.

Keywords: Cold gas thruster, I2T5, CubeSat propulsion, thermal analysis, heat transfer, thermal resistance, orbital heat fluxes.

Acknowledgements

"…be grateful every day for the brief, but magnificent opportunity that life provides."

- *Carl Sagan*

Yes, our lives are beautiful, meaningful and interesting, yet filled with challenges that test us in every manner possible. My journey hitherto has been an enthralling experience, for it is the people I've come across that have made my life wholesome, and more joyful. I am truly grateful to all these wonderful humans who have made a difference in my life, you know who you are.

I am grateful to Javier Martínez Martínez for agreeing to become my supervisor. His kind, calm and patient personality coupled with his knowledge and experience have been instrumental in shaping my thesis work. May the Schlieren force be with you!

I feel privileged to have been part of the ThrustMe team, who are like a family to me – Dr. Ane Aanesland, Dr. Dmytro Rafalskyi, Dr. Plamen 2020, Elena 2020 (Frozen Princess), Olena, les deux Antoines, Thomas, Laurène, Lui, Romain, Jérémy, Klinsman, Alice and Roy; thank you for your immense support, motivation and concern.

I am thankful to Dr. Victoria Barabash, Anette Snällfot-Brändström, Maria Winnebäck and the professors at LTU Rymdcampus, for offering their guidance, care and expertise during my time in Kiruna, Sweden. I thank Dr. Anita Enmark, Dr. Martin Hlinovský and Dr. Kristian Hengster-Movric for agreeing to examine my thesis work.

Throughout this master's course I have met some amazing souls, who I share a lot of interesting memories with – Niels, Mauro, Guillaume, Dr. Pokémon Max, Lucas, the Grönstensvägen 24 boys, Ehssan, Führer Max, Emanuele, Aydin, Javier, Guillermo, the Indian house, the Czech mates, well, the list goes on…but each and every one of them has made me smile.

I am eternally grateful to my parents for their blessings and for making me the person that I am today. I am super thankful to my sister, Ruth, and brother, Neville, for always having my back and inspiring me to be a better person. I am thankful to my love, Iryl, for being understanding, patient and for encouraging me always. All the love and care I've received from my relatives and friends in Mangalore and around the world has kept me motivated and peaceful, and I am really grateful to have them in my life.

Finally, I thank God for blessing me, for never leaving my side and for helping me get through this pandemic. His grace and everlasting love have kept me going strong.

Declaration

I, Roger Michael Pereira, hereby declare that I have elaborated this master thesis on my own, and that I have cited all the information sources that have been used, in accordance with the "Guideline No. 1/2009 for Adhering to Ethical Principles when Elaborating an Academic Final Thesis".

Place : Prague, Czech Republic

Date : August 14, 2020 Signature: …….

Contents

List of Figures

List of Tables

Chapter 1: Exordium

1.1 Introduction

With the onset of a technologically advanced era, the space industry is witnessing a paradigm shift from "bigger, stronger and better" to "smaller, robust and efficient". CubeSats are the embodiment of this very mindset. The CubeSat is a research spacecraft built to standard dimensions (called form factor or U), where 1U corresponds to a cube of size 10×10×10 cm, making it a class of nanosatellites [1]. Around 112 CubeSats were in orbit by 2012, since the first CubeSat launch in 2003 [2]. According to the nanosats database, the number of CubeSats launched has reached 1210, as of April 2020 [3]. CubeSats are gaining prominence as they are economical, reliable and open many pathways to access space directly. Their applications include (but not limited to) Earth remote sensing, academia, defence, atmospheric research, navigation and communication [4].

The popular choice of orbit for a CubeSat is the Low Earth Orbit (LEO), as it is relatively inexpensive to fly close to the Earth. However, the satellite will be subjected to space environmental effects like the Earth's atmospheric drag and physical sputtering (due to neutral molecules), outgassing (due to vacuum), surface charging (due to plasma interactions) and orbital debris [5]. These effects result in the de-orbiting of the satellite, and hence, the need for propulsion systems arises, to sustain the planned mission orbit.

Propulsion systems supplement the CubeSat by enabling active attitude control, drag recovery, orbital manoeuvring and extended mission lifetime [6]. These systems can be categorised as cold gas thrusters, electric propulsion systems, chemical propulsion systems and solar sails. A detailed explanation of the various propulsion systems can be found in [6], [7]. When choosing a suitable propulsion system, it is essential to keep in mind the following criteria – specific impulse required, thrust, size, weight, operational power, ΔV capacity of the thruster (to perform orbital manoeuvres), integration requirements (attachment to satellite), and reliability [4].

To address the need for sustainable propulsion systems for CubeSats, ThrustMe, France, has designed and developed a low-end propulsion system called the I2T5, that uses iodine as a solid propellant [8].

1.2 Description of the I2T5 Thruster

The I2T5 is a self-pressurised, iodine-propelled cold gas thruster. On November 3, 2019, the I2T5 carved a niche in the space industry by becoming the first ever iodine-based propulsion system to successfully reach space. Figure 1 shows the two different configurations of the I2T5 currently available in the market.

Figure 1: The I2T5 cold gas thruster in two different thrust configurations; front thrust (left), and side thrust (right) (Credits: Martínez et al. [8])

The I2T5 uses solid Iodine as a propellant, which sublimates at a rate proportional to the temperature [8]. The gas produced is then accelerated through a micro-nozzle. A flow control system is used to provide the desired gas flow rate at the exhaust. The thermal management system is responsible for maintaining the optimum temperature at the tank [8]. A schematic of the working of the I2T5 is shown in Figure 2.

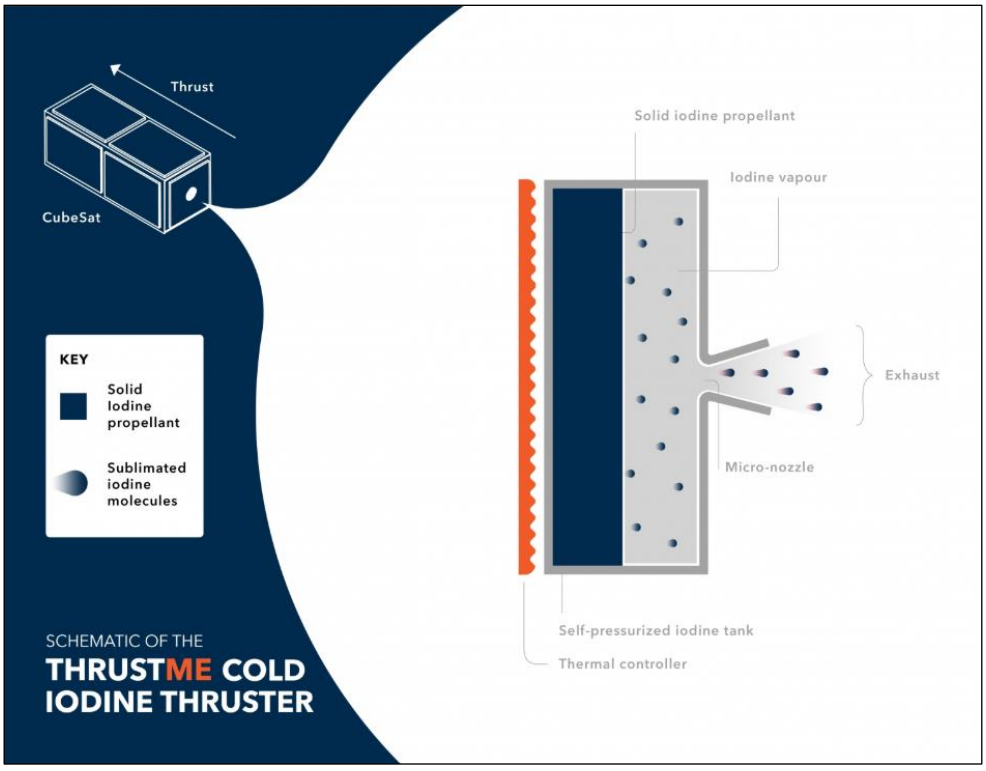

Figure 2: Functioning of the I2T5 (Credits: ThrustMe)

1.3 Motivation

The first flight measurements of the I2T5 showed that the thruster was functioning as expected [8]. There was, however, an issue encountered by the thermal management system, wherein, the tank was 6.5°C less than the optimum operating temperature [8]. Upon further inspection, it was observed that significant thermal contact existed between the propellant tank and the walls of the thruster frame. This affected the thrust obtained at the exhaust, as the warm-up time for the propellant tank increased [8]. Although this does not pose a major problem for the flight model, it is necessary to reduce the conduction heat loss to optimise future versions of the I2T5.

This thesis looks at improving the thermal performance of the I2T5 by reducing the total heat lost by the tank to the satellite frame, due to conduction only. Other sources of heat loss for e.g., due to radiation, are not studied in-depth. For the case of the I2T5, conduction losses are inevitable, and hence, must be considered for a proper thermal analysis. With limited power available for the thruster operation, it is important that the heat losses are kept to a minimum, if not zero.

1.4 Thesis Structure

Chapter 2 briefly looks at the importance of thermal control in satellites. The rest of the chapter is dedicated to understanding the basics of heat transfer, the thermal environment of space, and the radiative heat fluxes that result thereof. The information presented helps to initiate good thermal analyses. There are a plethora of sources that provide excellent pedagogical and industrial approaches to thermal simulations, but for this chapter, the main literature referred to are [9]–[15].

Chapter 3 is the crux of the thesis work. It begins with the assumptions made for the thermal simulations, and proceeds to explain the steps taken to alleviate the conductive heat loss in the I2T5. Following this, the observations made from an experiment performed on the I2T5 are mentioned. The chapter ends with a simulation on the environmental heat fluxes that the I2T5 will receive while in orbit.

Chapter 4 discusses the results obtained from the simulations and the experiment. A few plausible reasons for the discrepancies in data are mentioned.

Chapters 5 and 6 give the conclusion and future work that could be performed to thoroughly analyse the I2T5.

Chapter 2: Theoretical Background

This chapter is intended at providing the prerequisites for understanding the content in Chapter 3. The first section provides a brief introduction to thermal control. In the subsequent sections, the fundamentals of heat transfer are presented, along with an overview of the space thermal environment. As a majority of the thesis work relies on thermal simulations performed using COMSOL Multiphysics, the final section is dedicated to software functionality and accuracy.

2.1 Thermal Control

The thermal control subsystem is imperative for the smooth functioning of a spacecraft. This subsystem ensures that components within a spacecraft operate in their respective working temperature ranges.

There are mainly two types of thermal control – passive and active [16], [17]. Passive thermal control uses coatings, surface finishes, material properties (thermal conductivity, emissivity, etc) to sustain the desired temperature [16]. This type is simple, safe, inexpensive and does not consume any spacecraft resources [17]. Active thermal control uses thermo-electric coolers or heaters, sensing devices, heat exchangers to maintain the temperature [16]. This type is generally complex, hazardous, expensive and consumes electrical power [16], [17]. This thermal control is used when passive control systems cannot match the thermal requirements of a mission. As an example, in small structures with large power dissipation, like electronic components, that need to be operated at low temperatures, active thermal control is advantageous.

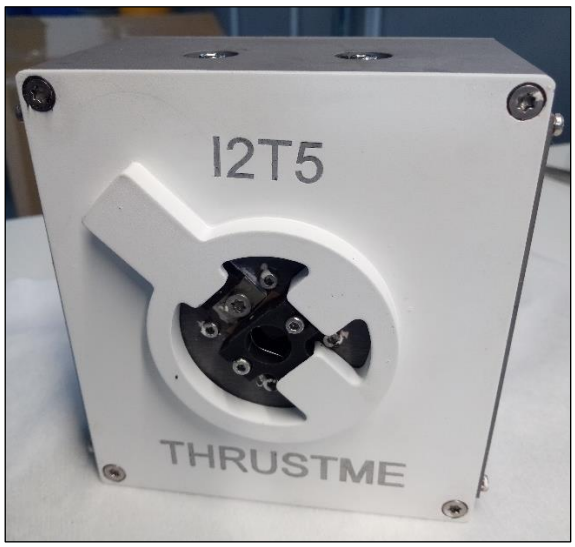

Figure 3: Passive thermal control in the I2T5 through surface radiation; the surface is painted to modify the emissivity (Credits: ThrustMe)

Figure 3 is an example of passive thermal control wherein, the radiating surface can be modified (by painting, anodising, polishing) to vary the surface emissivity. The material of the plate is highly conductive to facilitate faster heat flow.

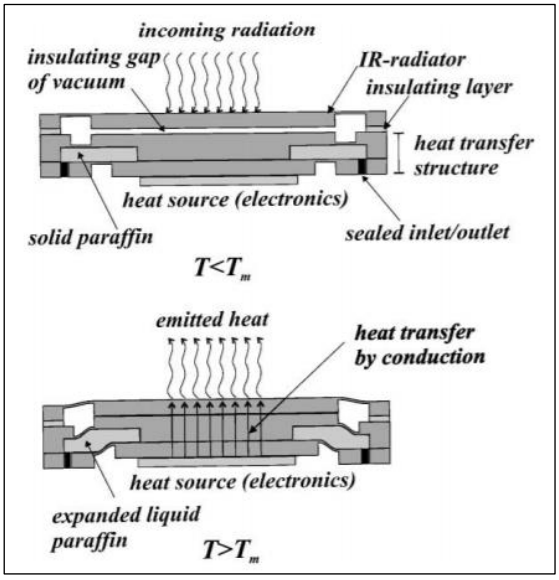

Figure 4: A paraffin phase transition actuator (*Credits: Klintberg et al.* [18])

Figure 4 is an example of an active thermal control method that could potentially be employed in nanosatellites [18]. The paraffin wax is the active element in this case. When the temperature of the component is low, the wax remains hard, but as the temperature increases, the wax melts, eventually conducting heat to the radiating surface [18]. In the figure, T_m is the melting point (65°C) of the paraffin wax used.

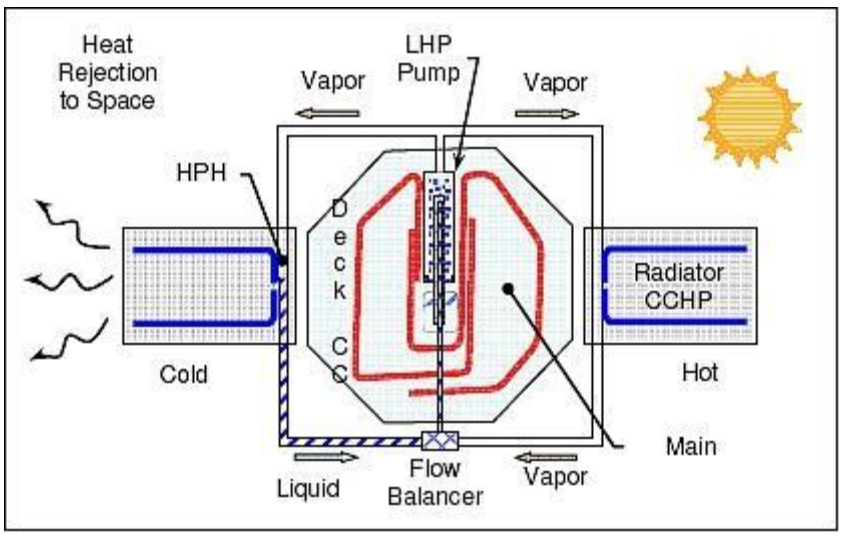

Figure 5: Thermal control system of the TacSat-4 (*Credits: Naval Research Laboratory* [19])

Figure 5 shows a schematic of the thermal control system of the TacSat-4, a tactical micro-satellite of the Naval Research Laboratory (NRL). The thermal control system uses an aluminium loop heat pipe (LHP) together with ammonia as the working fluid, to transmit heat from the electronics subsystem to the radiator sections [20]. In this case, both active and passive thermal control systems are employed.

2.2 Heat Transfer Mechanisms and their Couplings

There are three major modes of heat transfer – conduction, convection and radiation. Out of these, conduction and radiation are predominant in most space applications. Convection facilitates active thermal control, and is applicable to pressurised spacecraft (which are usually manned) [21]. Convective heat transfer systems help create an ambience within the spacecraft, that is conducive for human sustenance in space. Other applications include rocket boosters, fluid loops, and cryogenic cooling systems.

2.2.1 Conduction

This fundamental mode of heat transfer occurs between various spacecraft components physically linked to each other. By definition, conduction is the heat flux transported in a medium due to a temperature gradient, and this physical mechanism occurs at a molecular or atomic level [9]. Considering the case of the I2T5, this is the direct flow of heat from the propellant tank to the satellite frame, through the mechanical fasteners (bolts) and hardware (washers).

In all real systems, a temperature gradient causes the components to change from an initial state to a final state (thermal equilibrium). In between, the system is in a transient state, wherein the heating rate varies depending on the component material and geometrical properties. Conduction has two phases – transient and steady-state, which are explained below.

2.2.1.1 *Transient Conduction*

Any component (system) that is heated by conduction will first undergo a temperature rate of change, which in turn is used to calculate the heat flux. This is represented by the heat diffusion equation [9], [10], [12] as,

$$\boxed{\nabla^2 T + \frac{\dot{q}_v}{k} = \frac{1}{\alpha}\frac{\partial T}{\partial t}} \tag{1}$$

Where, $\nabla^2 T = \frac{\partial^2 T}{\partial x^2} + \frac{\partial^2 T}{\partial y^2} + \frac{\partial^2 T}{\partial z^2}$ and $\alpha = \frac{k}{\rho C_p} = \frac{Heat\ conducted}{Heat\ stored}$

T → Temperature [K] $\dot{q}_v$ → Heat generated/unit volume [W/m^3] k → Thermal conductivity [W/m-K] α → Thermal diffusivity [m^2/s]	t → Time [s] ρ → Density [kg/m^3] C_p → Specific heat capacity [J/kg-K]

To differentiate between transient and steady-state, take the following example. Consider a rod of length 10 cm and diameter 2 cm (Figure 6) which is initially at room temperature (20°C). One end of the rod (left) is kept at 50°C and the other end (right) has a temperature sensor. Using COMSOL Multiphysics, a transient thermal analysis was performed (time: 60 minutes) for two rod material cases – Aluminium 6082-T6 and Stainless Steel AISI 304, and the corresponding Temperature vs. Time graphs are shown in Figure 7 and Figure 8 respectively. The two materials were chosen as they are currently equipped for the I2T5.

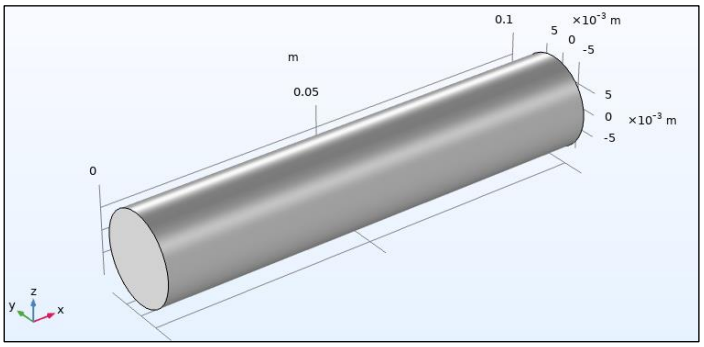

Figure 6: Solid rod (modelled in COMSOL) for transient conduction analysis

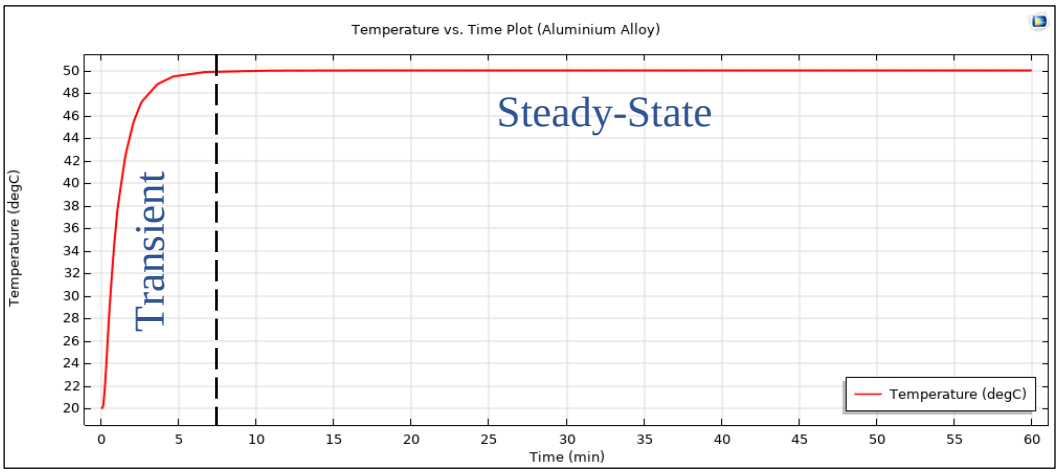

Figure 7: Temperature vs. Time plot for the aluminium alloy rod; a clear distinction is seen between the transient and steady-state regions

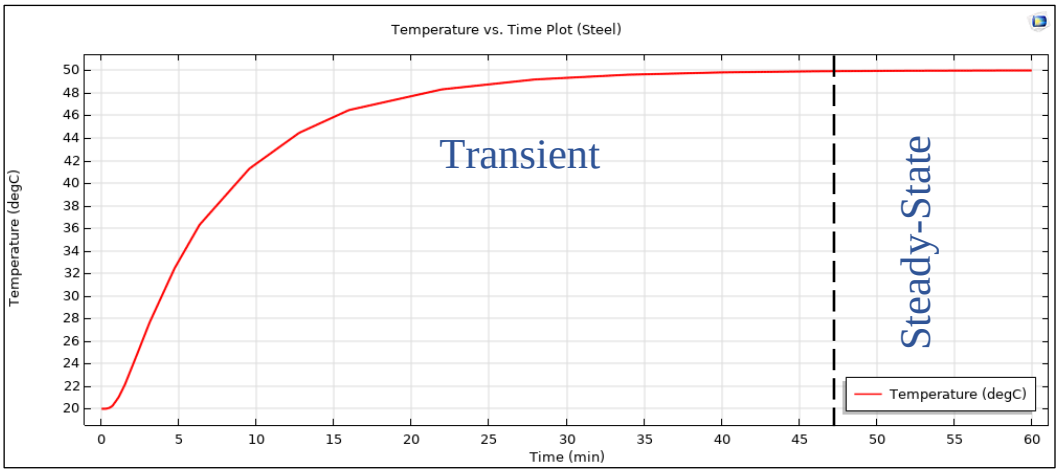

Figure 8: Temperature vs. Time plot for the stainless-steel rod

Comparing the two figures above, it is evident that the transient time in the aluminium alloy rod case is much less than that of the stainless-steel rod case. This is because aluminium has a higher thermal diffusivity than steel. A high diffusivity value implies that the rate of heat conduction is larger than the rate of heat stored (refer equation (1)), resulting in the material achieving steady-state faster.

2.2.1.2 *Steady-State Conduction*

Any system that is in thermal equilibrium with its surroundings is in a condition of steady-state. Mathematically, this implies that the term on the RHS of equation (1) goes to zero, and the following equation is obtained [9], [10],

$$\boxed{\dot{q}_v = -\mathrm{k}\,\nabla^2 T} \tag{2}$$

Although conductive heat transfer is three dimensional, for simplicity, one dimensional heat flow is usually considered, which yields accurate results. Assuming that the conduction is in one direction, and that there is no heat generation, equation (2) becomes [9], [10],

$$\boxed{\frac{d}{dx}\left(k\frac{dT}{dx}\right) = 0} \tag{3}$$

Solving equation (3) yields a familiar equation called the Fourier's law for 1-D conduction, which is,

$$\boxed{Q_{cond}\,[W] = -kA\frac{dT}{dx} = -kA\frac{(T_1 - T_2)}{L}} \tag{4}$$

T_1, T_2 → Surface temperatures [K], with $T_1 > T_2$ A → Cross-sectional area [m^2]	k → Thermal conductivity [W/m-K] L → Thickness [m]

2.2.2 Convection

This mode of heat transfer occurs due to two mechanisms – diffusion, and the macroscopic motion of the fluid [9]. By definition, convection is the transfer of heat in a system due to fluid flow, which causes a temperature gradient at the boundaries. Figure 9 shows this process. Convection is classified as forced convection, and free convection [9].

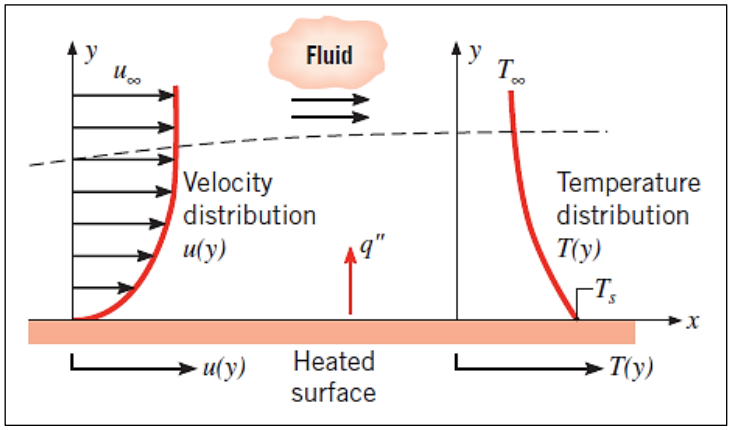

Figure 9: Convective heat transfer at the boundary (Credits: Bergman et al. [9])

In mathematical terms, the heat flux due to convection is given by Newton's law of cooling as,

$$Q_{conv}[W] = hA(T_s - T_\infty) \tag{5}$$

T_s → Surface temperature [K] T_∞ → Fluid temperature [K]	h → Convection heat transfer coefficient [W/m^2-K] A → Cross-sectional area [m^2]

The heat transfer coefficient, *h*, is dependent on the boundary layer conditions. Factors like fluid thermodynamics and transport properties, surface geometry, and nature of fluid flow affect the conditions at the boundary [9].

2.2.3 Radiation

This mode of heat transfer occurs irrespective of the intervening medium. By definition, it is the heat emitted by a body at a finite temperature, to the surroundings [9]. The surroundings could mean the ambient or other bodies. The former type is called surface-to-ambient radiation, and the latter, surface-to-surface radiation.

Although radiation can occur from fluids, this thesis only regards radiation from solids. Fluid radiation is a volumetric phenomenon, and finds its application in studying the behaviour of lenses [12].

Figure 10 illustrates the radiative heat transfer process between a solid and its surroundings. If $T_s > T_{sur}$, then the net radiative flux is towards the surroundings, and if $T_s < T_{sur}$, the net radiative flux is towards the body in question.

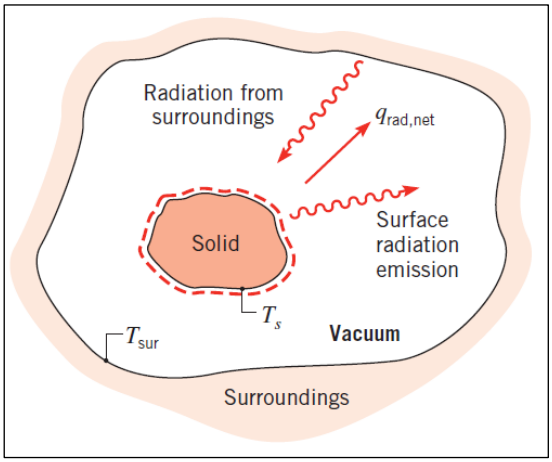

Figure 10: Radiative heat transfer from a solid to its surroundings (*Credits: Bergman et al.* [9])

Thermal radiation falls within the electromagnetic spectrum, and the range of wavelength is from 0.1 µm to 100 µm (refer Figure 11). This implies that thermal radiation is constituted by partial ultra violet, complete visible and infrared waves [9], [10], [12].

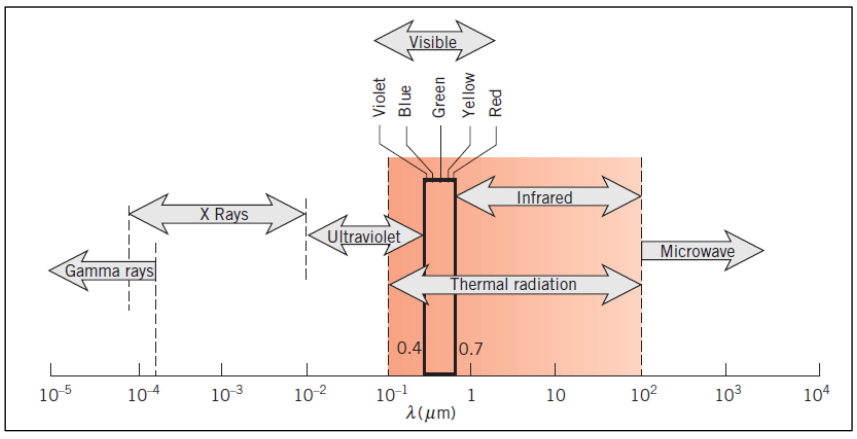

Figure 11: Thermal radiation in the electromagnetic spectrum (*Credits: Bergman et al.* [9])

The heat radiated from a surface is a function of the temperature and surface properties, and is given by the Stefan – Boltzmann law for grey bodies as,

$$\boxed{Q_{rad}[W] = \varepsilon A \sigma T_s^4} \tag{6}$$

T_s → Surface temperature [K] σ → Stefan-Boltzmann constant, $5.67 \times 10^{-8}\ [W/m^2.K^4]$	A → Surface area [m^2] ε → Surface emissivity

The surface emissivity, ε, lies between 0 and 1 for grey bodies, and is equal to 0 for an ideal white body (perfect reflector), and has a value of 1 for an ideal blackbody (perfect emitter). This value depends on the surface finish and material [9].

2.3 Thermal Circuits and Resistances

Thermal resistance is the resistance that a material offers to the flow of heat [10], and is dependent on the geometry and thermal conductivity of the component considered. Any complex system can be modelled as a network of thermal resistances. This gives a clear picture on the flow of heat from one point to another. Table 1 presents some similarities between thermal and electrical circuits.

Table 1: The analogy between electrical and thermal circuits

	Electrical Circuit	**Thermal Circuit**
Driving Force	Voltage or Potential Difference, $\Delta V\ [V]$	Temperature Gradient, $\Delta T\ [K]$
Flow	Current, $I\ [A]$	Heat Flux, $Q\ [W]$
Resistance to Flow	Electrical Resistance, $R\ [\Omega] = \frac{\Delta V}{I}$	Thermal Resistance, $R_{th}\ [K/W] = \frac{\Delta T}{Q}$
Conductivity	Electrical Conductivity, $\sigma\ [S/m]$	Thermal Conductivity, $k\ [W/m.K]$
Resistivity	Electrical Resistivity, $\rho\ [\Omega.m] = \frac{1}{\sigma}$	Thermal Resistivity, $R_\lambda\ [m.K/W] = \frac{1}{k}$

For the case of the I2T5, conduction and radiation are predominant, and hence, will be the focus of this section. Generally, developing a conductive thermal circuit for a multi-body system is feasible. However, the complexity of the radiative thermal circuit for such a system increases with an increase in the number of surfaces.

The concept of thermal resistance has its limitations, wherein, it can only be considered for a system at steady-state, having no internal heat generation, and the heat transfer is one-dimensional [10].

2.3.1 Conduction Thermal Circuit

For a 1-D, steady-state system, the conductive resistance is given by,

$$\boxed{R_{cond}\,[K/W] = \frac{\Delta T}{Q} = \frac{L}{kA} = \frac{1}{kS}} \tag{7}$$

Where, $S = \frac{A}{L}$, is the Langmuir conductive shape factor. This term is useful for estimating the conductive heat flux through slightly complex 2-D and 3-D geometries. [11], [22]

Consider the steady-state composite slab in Figure 12, where the left end is at temperature T_1 and the right end is at temperature T_4 (note that, $T_1 > T_4$). The term, Q, is the heat flux through the slab. This is a purely conductive system, and is a combination of parallel and series resistances.

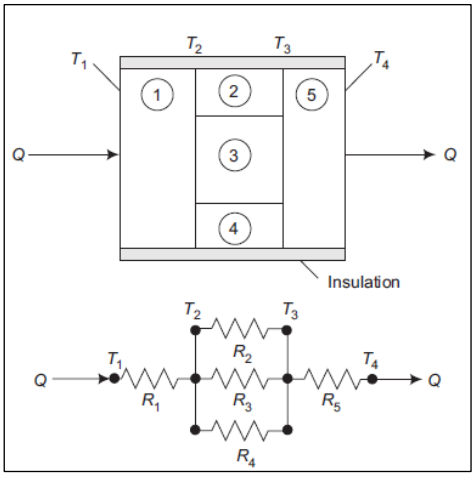

Figure 12: A composite slab [top] and the equivalent thermal circuit consisting of series-parallel resistances [bottom] (Credits: Thirumaleshwar, M. [10])

The thermal circuit of the system can be evaluated as follows,

For the parallel resistors: $R_{2,3,4_{eff}} = \left(\frac{1}{R_2} + \frac{1}{R_3} + \frac{1}{R_4}\right)^{-1}$

This is in series with the R_1 & R_5 resistors, hence, they can be added to obtain the effective resistance as follows,

$$R_{eff} = R_1 + R_{2,3,4_{eff}} + R_5$$

Using equation (7) to calculate the heat flux: $Q\,[W] = \frac{T_1 - T_4}{R_{eff}}$

2.3.2 Radiation Thermal Circuit

Consider a grey, diffuse and opaque surface, i, at a temperature, T_i, having surface emissivity, ε_i, and surface absorptivity, α_i. The net radiation exchange at the surface is given by the following equation [9],

$$\boxed{Q_{rad_i}\,[W] = A_i(J_i - G_i) = A_i(\varepsilon_i \sigma T_i^4 - \alpha_i G_i)} \tag{8}$$

$A_i \rightarrow$ Surface area $[m^2]$
$J_i \rightarrow$ Radiosity $[W/m^2]$
$G_i \rightarrow$ Irradiation $[W/m^2]$

The term Radiosity refers to the rate at which radiation leaves a surface per unit area, whereas, Irradiation is the rate at which radiation is incident on a surface per unit area (Figure 13). The sources of irradiation are: ambient (due to the surrounding temperature), external (thermal environment of space; refer section 2.4) or radiation from other surfaces.

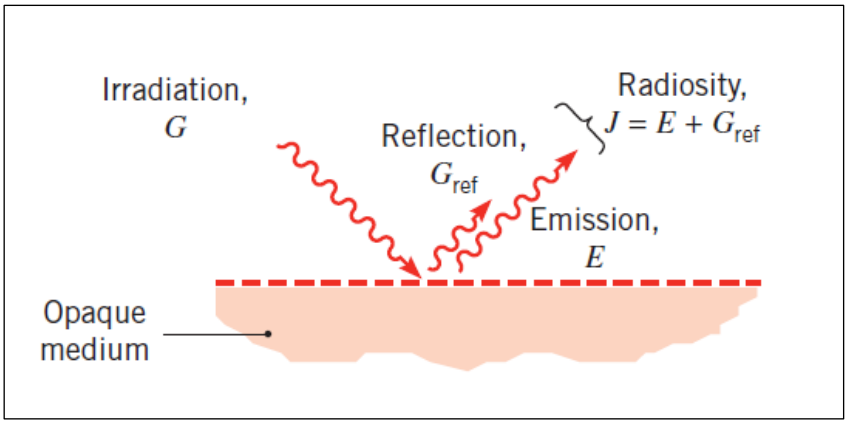

Figure 13: Radiation for an opaque surface (Credits: Bergman et al. [9])

In an enclosed system, a surface will radiate to both, the ambient, and to another surface, or either of the two. The generalised thermal circuit for such a three-way radiative system is illustrated in Figure 14.

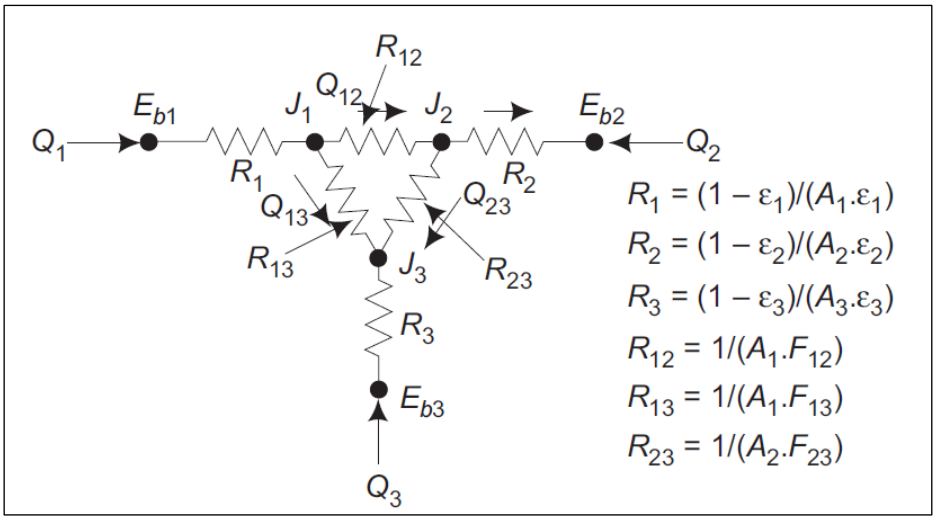

Figure 14: A three-way thermal radiative circuit for an enclosure (*Credits: Thirumaleshwar, M.* [10])

To generalise the above figure, for an N-surface enclosure with view factors, F_{ij}, net radiative heat exchange, Q_{ij}, the radiative flux balance at any node, J_i, yields the following relation [9], [10],

$$Q_i = \frac{E_{b_i} - J_i}{\left(\frac{1-\varepsilon_i}{A_i \varepsilon_i}\right)} = \sum_{j=1}^{N} \frac{J_i - J_j}{\left(\frac{1}{A_i F_{ij}}\right)} = \sum_{1}^{N} Q_{ij} \tag{9}$$

Where, $R_i = \frac{1-\varepsilon_i}{A_i \varepsilon_i} \rightarrow$ Surface Resistance and $R_{ij} = \frac{1}{A_i F_{ij}} \rightarrow$ Space Resistance

2.4 The Thermal Environment of Space

For a spacecraft, either orbiting a planet, or on an interplanetary mission, there is always an external source of heating that occurs due to the electromagnetic radiation from the sun, or other planets. Also, during launch and at very low orbits (rarefied atmosphere), the spacecraft is affected by free molecular heating due to friction [13].

At low-earth orbits, a spacecraft is exposed to a small portion of the Earth at a given time. If the space vehicle is large and well-insulated, no drastic effects occur even if the thermal environment changes rapidly. However, exposed sensitive components such as solar arrays, will be affected by small changes [13]. Hence, the thermal environmental effects have to be considered when designing sensitive components.

2.4.1 Direct Solar Irradiation

This is the total heat flux that a spacecraft receives due to the electromagnetic radiation from the sun. The magnitude of flux depends on the surface absorptivity and also, the orientation of the spacecraft with respect to the solar vector. The solar radiation is made up of short wavelengths, and is quite energetic due to the temperature of the sun, which is assumed to behave like a black body radiating heat at 5800 K [9].

The solar flux that is directly received from the sun is termed as the Solar Constant (S_c) [14]. This is estimated to vary between 1365 and 1373 $\mathrm{W/m^2}$ just above the Earth's atmosphere, and at a mean distance from the sun. During the summer and winter solstices, the value of the solar constant varies between $1310 \pm 10\ \mathrm{W/m^2}$ and $1390 \pm 10\ W/m^2$, respectively [14]. Generally, a value of $1350 \pm 2\ \mathrm{W/m^2}$ is assumed for calculations [14].

To determine the direct solar irradiation on a spacecraft surface, i, the following formula is used [15],

$$\boxed{Q_{solar_i} = \alpha S_c A_i \cos(\theta_i)} \tag{10}$$

A_i → Surface area [m^2]	S_c → Solar constant [m^2]
α → Surface absorptivity	θ_i → Angle between the surface normal and the solar vector [rad]

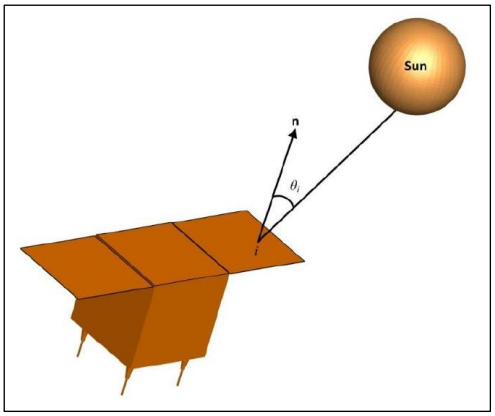

Figure 15: Orientation of a satellite surface, i, with respect to the sun (Credits: Uygur, A. [15])

If the satellite moves into Earth's shadow, then the direct solar flux does not reach the surface. This effect has to be taken into account for a thorough orbital analysis.

2.4.2 Planetary Infrared Irradiation

This is the incident solar radiation that is reemitted by a planetary body as infrared (IR) energy. The amount of radiation that is emitted depends on the location, for e.g., a warmer region (deserts, tropics) would radiate more heat than a colder region (poles) [13].

The effective temperature of Earth is about -18°C (255.15 K), and it emits longwave radiation (generally, $\lambda > 4\ \mu m$) in contrast to the shortwave solar radiation [13]. Since longwave radiation is also emitted by a spacecraft, the emissivity of the surface in the IR spectrum becomes an important factor to determine the total Earth flux to the surface. For thermal analysis, a nominal value of the Earth IR flux is used, which is about $236\ W/m^2$ [14].

The Earth infrared flux can be calculated as follows [15],

$$\boxed{Q_{Earth,IR_i} = \varepsilon_{IR_i} A_i F_{i\to Earth} \sigma T_E^4} \tag{11}$$

A_i → Surface area [m^2] ε_{IR_i} → Surface emissivity in the IR spectrum	σ → Stefan-Boltzmann constant [$W/m^2.K^4$] T_E → Surface temperature [K] $F_{i\to Earth}$ → View factor from surface to Earth

2.4.3 Planetary Albedo Irradiation

This is the solar flux that is reflected off a planetary body. The magnitude of this heat flux depends on the planetary albedo, which is defined as the fraction of the total incident solar energy that is reflected back into space [13], [23]. Although the albedo varies seasonally and geographically, a good approximation for the albedo of Earth is 0.36 [24].

The planetary albedo irradiation on a spacecraft surface is given by [15],

$$\boxed{Q_{Alb_i} = a S_c \alpha A_i F_{i\to Earth} \cos(\beta_i)} \tag{12}$$

A_i → Surface area [m^2] a → Albedo coefficient	β_i → Angle between the vectors joining the Earth to the surface normal and to the sun respectively [rad]

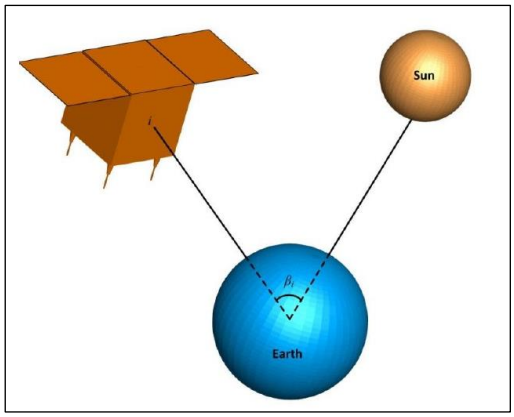

Figure 16: A view of the beta angle which controls the albedo flux heating (Credits: Uygur, A. [15])

The value of the albedo irradiation decreases as a spacecraft traverses its orbit and away from the subsolar point (a point where the Sun is at the zenith of a planet) [13], [14]. This decrease depends on the cosine of the beta angle (Figure 16). When the spacecraft enters the eclipse region of a planet, the albedo flux heating reaches zero, and this occurrence has to be accounted for, during orbital analysis. [13]

2.5 Balance of Heat Fluxes

To design a thermally stable spacecraft, it is important to understand the temperatures that each of the surfaces will reach during a mission. This is achieved by performing a heat balance study of the spacecraft as follows.

Consider a spacecraft surface as shown in Figure 17. There are four major sources of heat input – solar heating ($\dot{Q}_{solar}$), albedo heating ($\dot{Q}_{albedo}$), earth infrared heating ($\dot{Q}_{earth_{IR}}$), and internal energy dissipation ($\dot{g}$) due to the onboard electronics & system configuration. [11]

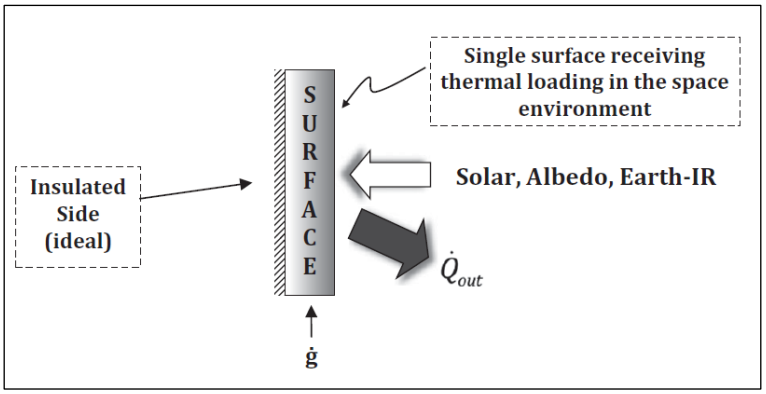

Figure 17: Spacecraft surface for heat balance study (Credits: Silk, E. [11])

From the law of conservation of energy, thermal equilibrium is reached when the heat rejected by the satellite surface due to radiation ($\dot{Q}_{out}$) is balanced by the external and internal energy loads as follows [11],

$$\boxed{\dot{Q}_{out}\,[W] = \dot{Q}_{ext} + \dot{Q}_{int} = \left(\dot{Q}_{solar} + \dot{Q}_{earth_{IR}} + \dot{Q}_{albedo}\right) + (\dot{g})} \tag{13}$$

The heat rejected to the space environment is purely through radiation, and hence, the Stefan-Boltzmann law for grey bodies is applicable [11].

2.6 The Working of COMSOL

The simulations for this thesis were performed using the Heat Transfer Module offered by COMSOL Multiphysics. This software uses the Finite Element Method to analyse, solve and simulate Multiphysics environments. It is powerful, user-friendly, transparent, reliable, accurate, and has a moderate learning curve for new users.

The results obtained using this software are sufficiently accurate and comparable to other simulation platforms like ANSYS, as depicted in a study by Salvi et al [25]. The reliability of the software to use numerical methods to solve problems is determined in a study by Vajdi et al. [26]. Although COMSOL uses significant memory, it is quite flexible with the modelling environment, which facilitates efficient computation. The accuracy of COMSOL to compute radiative view factors has been studied in Appendix – B, which is important for the accurate calculation of radiosities and radiative heat fluxes.

2.6.1 Radiative View Factor

One of the most prominent terms in surface-to-surface radiation is the view factor. The radiative view factor is the fraction of radiant energy that leaves one surface, i, and strikes another surface, j, directly [9], [10], [27]. It is also referred to as shape factor/configuration factor/angle factor. Reflection or re-radiation is not considered in the calculation of the view factor.

Consider two surfaces, A_i and A_j, having uniform radiosity and elemental areas, dA_i and dA_j, as shown in Figure 18. The line joining the respective normals, n_i and n_j, is of length, R. This line makes angles, θ_i and θ_j, respectively, with the two normals. The term, $d\omega_{ji}$, is the solid angle subtended by dA_j when viewed from the perspective of dA_i [9].

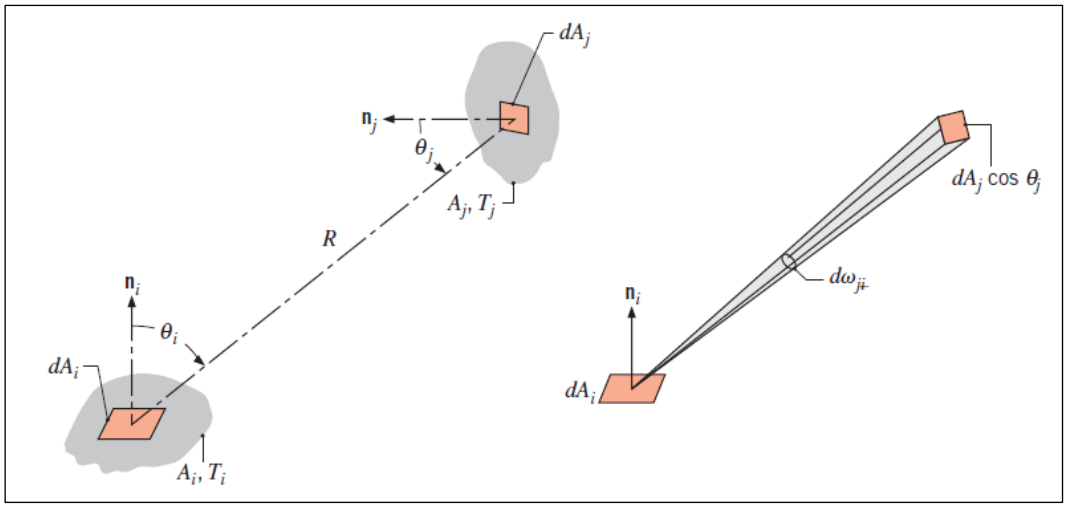

Figure 18: The concept of radiative view factor and its associated terms (*Credits: Bergman et al.* [9])

The view factor, F_{ij} or $F_{i\to j}$, is given by [9],

$$\boxed{F_{ij} = \frac{1}{A_i}\int_{A_i}\int_{A_j}\frac{cos\theta_i\, cos\theta_j}{\pi R^2}\, dA_i\, dA_j} \qquad (14)$$

Chapter 3: Methodology and Results

The primary focus of this thesis is to optimise the existing design of the I2T5 to improve its thermal performance. This would mean modifying the configuration, employing different materials for the components, or changing the geometry of specific components.

A step-by-step method is presented in this chapter, to cover every possible aspect of optimisation, under the given constraints. The objective is to decrease the effective thermal conductance (reduce the heat flux) between the tank of the I2T5 and the satellite frame. Some of the optimisation constraints are: the tank temperature has to be maintained at 100°C, limited input power to the thruster (5-20 W), the satellite frame temperatures vary between -20°C to +30°C.

The first section of this chapter is a brief overview of the assumptions made to simplify the study. The subsequent sections provide a logical procedure to alleviate the conductive heat loss problem of the I2T5.

3.1 Assumptions

The thermal modelling of a thruster can be complex (due to the geometry or physics involved), and this results in a computationally intensive analysis. Hence, specific assumptions have been made to facilitate optimum simulations.

First, the I2T5 is assumed to be perfectly integrated to a CubeSat maintained at 0°C. Second, the thruster internal radiation is small compared to the conduction. Third, there is perfect contact between the various components of the I2T5, and hence, the thermal contact resistance can be neglected. Fourth, the radiation analysis is performed assuming the ambient temperature as approximately 2.7 K, which has been measured as the temperature of the cosmic microwave background [28]. Fifth, the thermal conductivity, k [W/m.K], does not vary with temperature and time (since the range of temperatures considered is small). Sixth, surface erosion effects due to the iodine propellant are not considered. Seventh, space environmental effects such as micrometeoroid/orbital debris, contamination, sputtering are not considered, and hence, surface properties such as emissivity and absorptance remain constant with time.

3.2 **(Step 1)** Perform a Preliminary Analysis of the I2T5

Using the COMSOL Heat Transfer module, a preliminary thermal analysis of the I2T5 was conducted to gain a better perspective of the conductive heat flux distribution. A simplified model (thermal model) of the I2T5 (Figure 19) was used to reduce the computation time while ensuring minimum deviation from the original thruster design.

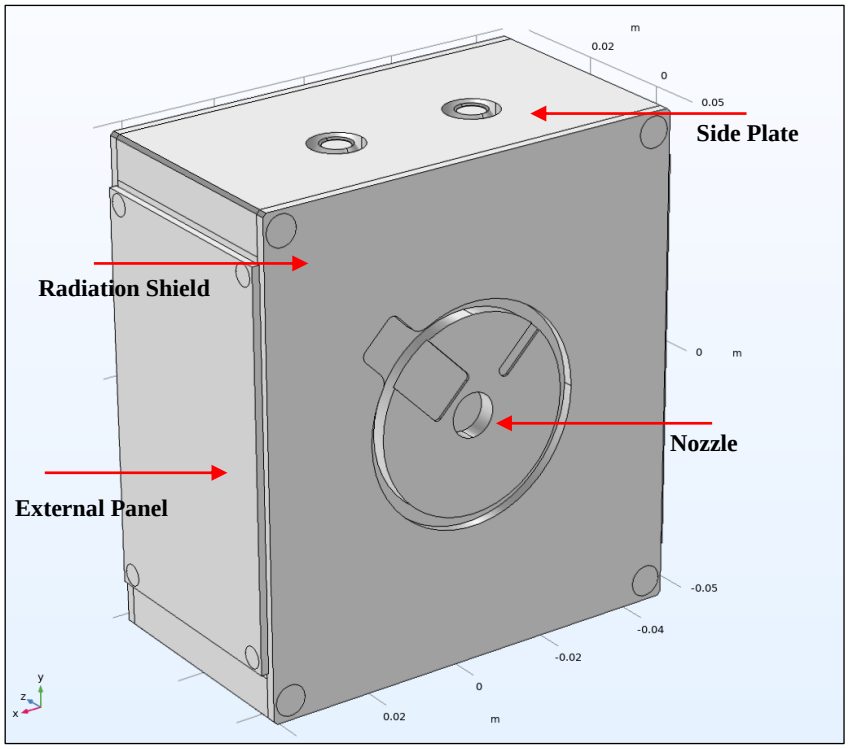

Figure 19: The CAD model of the I2T5, showing the nozzle, side plate, external panels and radiation plate (Credits: Antoine Poyet, ThrustMe)

For the analysis, a parametric study is performed with the system at steady-state. The tank and the makeshift satellite frame (Figure 20) are maintained at 100°C, and {-20°C, 0°C, 20°C} respectively, to account for the different scenarios that could occur while the thruster is in orbit.

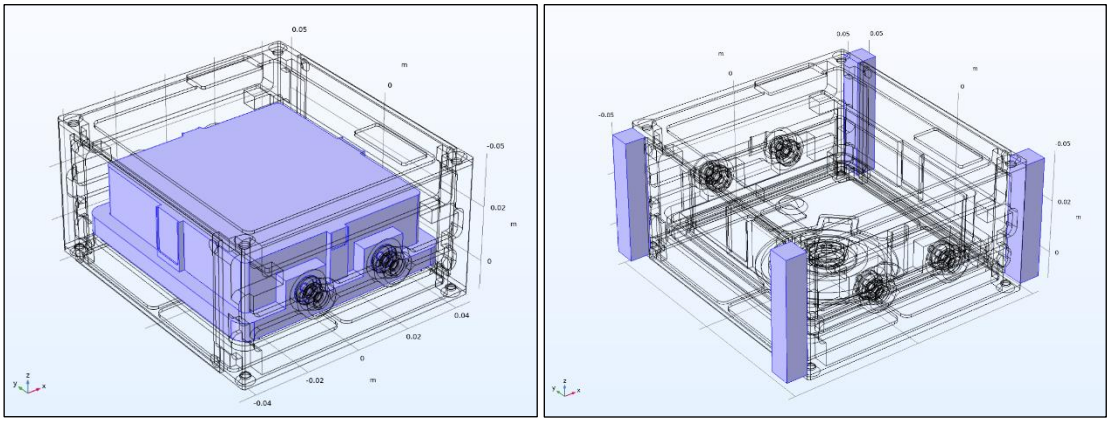

Figure 20: (Highlighted in blue) A 3-D view of the I2T5 tank (left) and the makeshift satellite frame (right)

The fluxes displayed in Table 2 lay the foundation upon which the I2T5 will be optimised to get lower heat flux values at the satellite frame.

Table 2: Total heat loss at the satellite frame for the base model

Tank Temperature [°C (K)]	Satellite Frame Temperature [°C (K)]	Heat Loss at the Satellite Frame [W]
100 (373.15)	-20 (253.15)	2.60
	0 (273.15)	2.16
	20 (293.15)	1.72

With the conductive fluxes and the temperatures known, it is possible to calculate the thermal resistance (K/W or °C/W) of the various thruster components. The thermal circuit for the I2T5 is developed, as shown in Figure 21 below. The conduction mainly occurs in the direction of the contact-normal between two adjacent components. Hence, a simplified, 1-D conduction model is assumed.

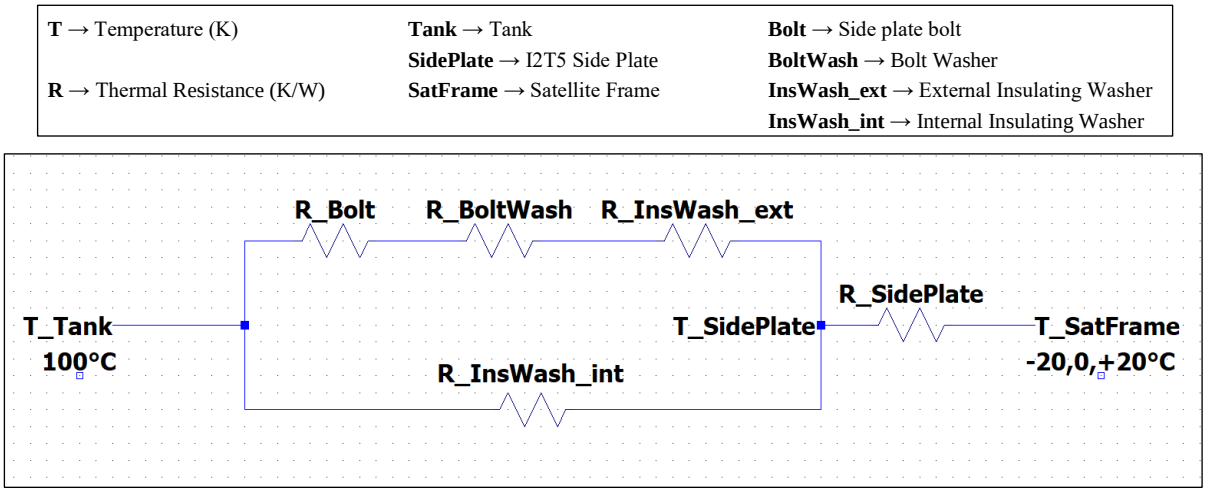

Figure 21: Conductive thermal circuit for the I2T5 thruster

It was observed that the flux distribution in the I2T5 is symmetric, and mainly occurs on the side plates. Hence, the initial thermal model (Figure 19) was reduced to analysing just one of the side plates (Figure 23), significantly reducing meshing and computation time. The results were then extrapolated to the entire thruster. A view of the washer-bolt configuration which will be thoroughly analysed is illustrated in Figure 22.

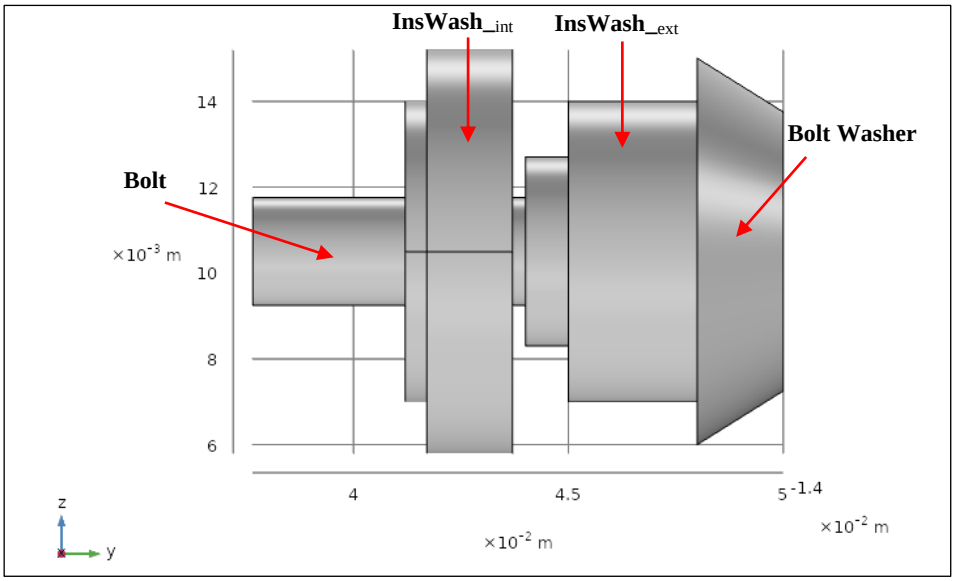

Figure 22: Side view of the Washer-Bolt configuration

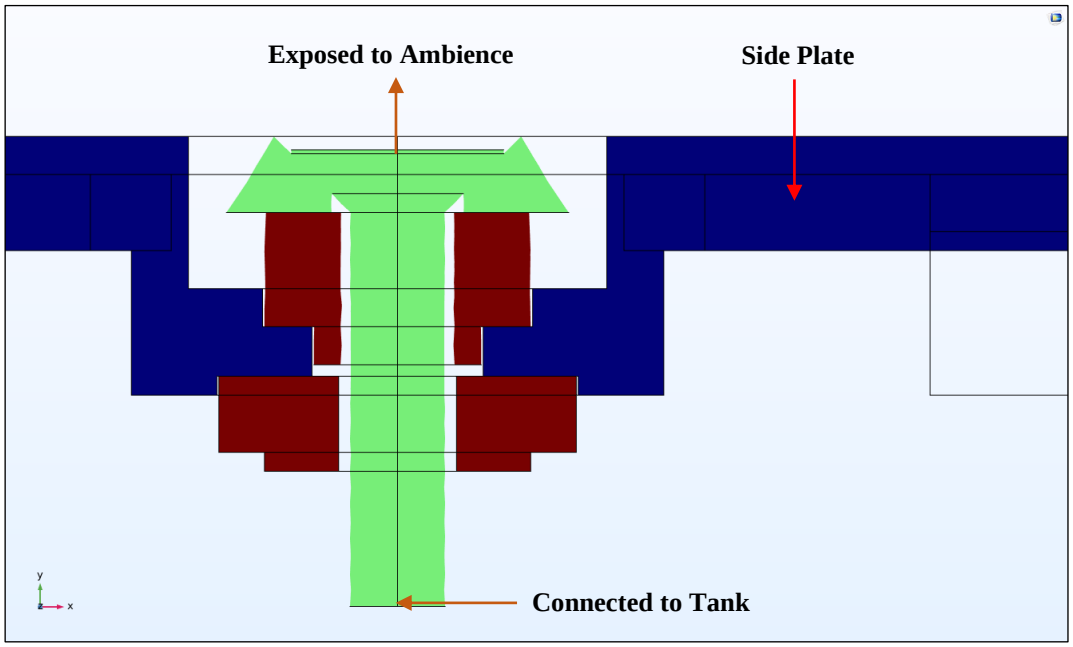

Figure 23: Cross-sectional view of the Washer-Bolt configuration attached to the I2T5 side plate

3.3 **(Step 2)** Identify the Scope of Improvement

From the preliminary analysis, it was identified that the heat loss mainly occurs through the side plates of the I2T5. A closer look at the data reveals that the washer-bolt configuration controls a major portion of the total heat flux from the tank to the satellite frame, with a minor contribution from external and internal radiating surfaces of the I2T5. To visualise this heat flow and also the temperature gradient, the black vectors in Figure 24 are used. Note that the vectors are scaled-down to maintain the clarity of the figure.

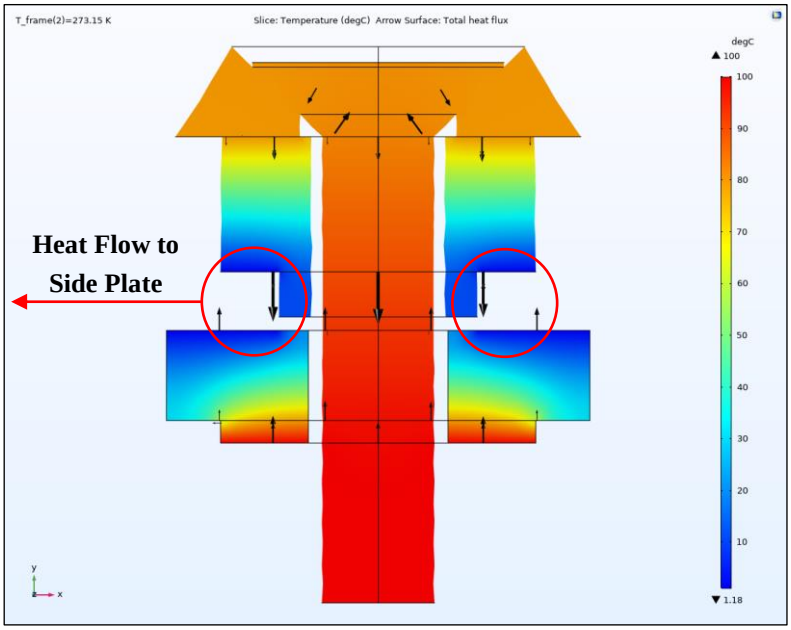

Figure 24: Temperature slice of the Washer-Bolt configuration; the direction of heat flow is shown by the arrows

From the above figure, it is evident that the insulating washers (material: Polytetrafluoroethylene or PTFE) offer excellent thermal resistance to the heat flow. This thermal resistance, however, can be increased by using materials with lower thermal conductivities (e.g., thermoplastics).

Finally, considering all possibilities, three potential areas of improvement were identified – material, design and configuration. Each of these modifications is discussed in detail in section 3.4 below.

3.4 **(Step 3)** Implement the Potential Modifications to the I2T5

The main criteria considered for making the right modifications (design, material or configuration) is that the conductive flux obtained at the satellite frames is reduced. The thruster receives limited power as input, and any power going to the frame is considered a loss. A significant portion of the input power is used to heat the tank to the operating temperature to sublimate the iodine (solid propellant) contained within. By reducing the

power loss at the frame, the tank will heat faster and the transient heating time is significantly decreased, which in turn will improve the thruster performance.

Concomitant with a low steady-state flux is a lower average temperature on the side plates of the I2T5, resulting in reduced surface-to-ambient radiation. Minimum radiation of the side plates is desirable, as the primary thermal control happens through the radiation plate. The following subsections provide an overview of the feasible modifications made to the I2T5 to decrease the thermal conductance between the tank and the satellite frame.

3.4.1 Change in Material

From Fourier's Law (section 2.2.1), the thermal conductivity or 'k' (W/m-K) term is dependent on the material. To reduce thermal conductance, materials with low 'k' values have to be used. It is important that these materials have low outgassing values and a total mass loss (TML) < 1% when exposed to the vacuum of space [29]. Also, these materials need to possess good mechanical properties (fatigue and yield strength, toughness, stiffness, etc.) to resist the shocks and vibrations during a rocket launch. An extensive treatment on the outgassing of space-grade materials can be found in [30], [31].

Insulating washers are utilised in the I2T5 to decrease heat loss. Simulations were run using various commercially available materials (refer Appendix – A), for the insulators and the side plates, and the results are tabulated below (Table 3). All simulations were run with a tank temperature of 100°C and a satellite frame temperature of 0°C.

Table 3: Total heat loss at the satellite frame for various combinations of materials

Case No.	**Material**				**Total Heat Loss [W]**
	Side Plate	***Bolt***	***Bolt Washer***	***Insulating Washers***	
1	SS	SS	SS	PTFE	**2.1604**
2	SS	SS	SS	PEEK	**2.0052**
3	SS	SS	SS	Polycarbonate	**1.7321**
4	Ti 6Al-4V	SS	SS	Polycarbonate	**1.4603**
5	Ti 6Al-4V	Ti 6Al-4V	Ti 6Al-4V	Polycarbonate	**1.3907**

In the table above, case 1 represents the base model that has to be improved. For case 2, PEEK insulating washers were chosen, which reduced the heat loss by 7.2%. As for polycarbonate insulating washers in case 3, the heat loss was reduced by 19.8%. For cases 4 and 5, the material of the insulating washers was kept constant, whereas the side plate

material was chosen to be a Titanium alloy, instead of stainless-steel (SS). This brought down the total heat loss by 32.4% and 35.6%, respectively, for cases 4 and 5.

3.4.2 Change in Geometry

Another way to increase the thermal resistance between the tank and the satellite frame is to reduce the surface area, or increase the thickness of the components. For the I2T5, this can be achieved by cutting slots on the washers, or by increasing the thickness of the insulating washers.

The current physical model of the I2T5 introduces another constraint wherein, the distance between the tank and the side plate should remain fixed. Therefore, increasing the thickness of the insulating washers could mean reducing the dimensions of the propellant tank, and consequently, the solid iodine available for propulsion. To avoid affecting the tank, the insulating washers were modified by creating slots to reduce the surface area available for conduction. The changes are shown in Figure 25 and Figure 26. The shape of the slots was chosen so as to remove as much material as possible without compromising the integrity (bearing strength, rigidity) of the washers. The slots are shaped equally to balance the radial stresses that arise due to compressive loading (tightening of screws).

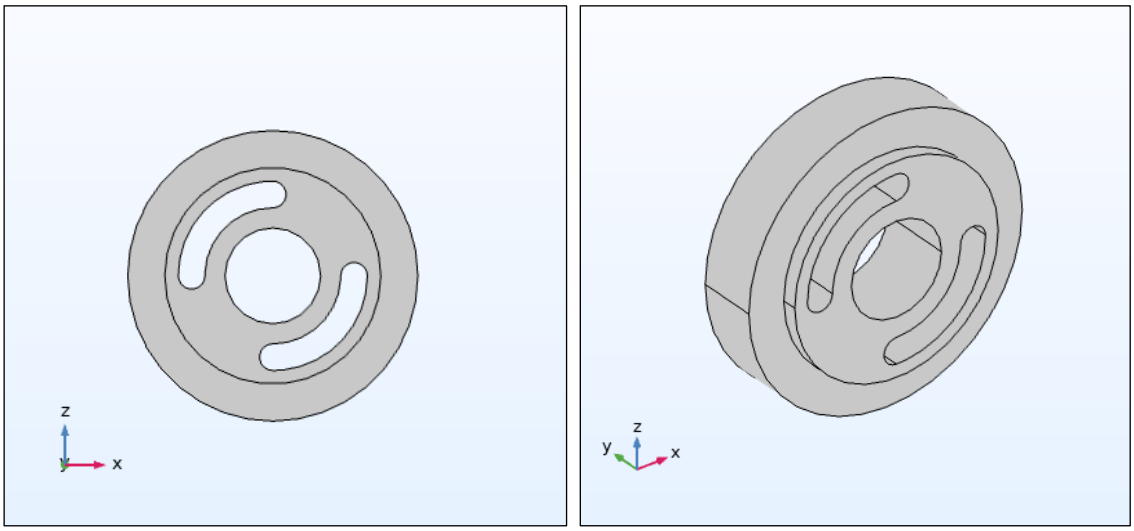

Figure 25: Slots made on the internal insulating washers; front view (left) and isometric view (right)

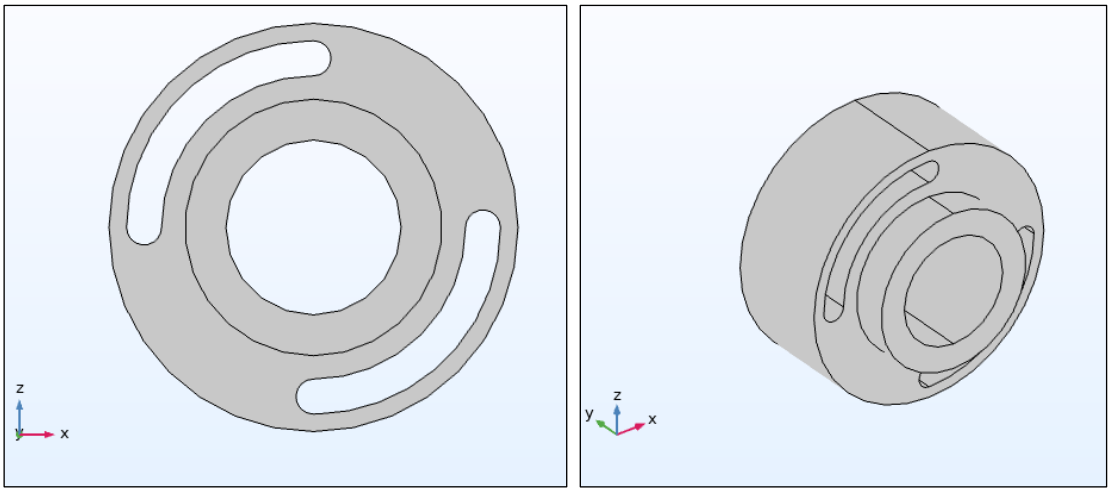

Figure 26: Slots made on the external insulating washers; front view (left) and isometric view (right)

The total heat loss at the frame was analysed using the same simulation conditions as in section 3.4.1, and in addition to geometry modification, different material combinations were analysed. The results are tabulated below (Table 4).

Table 4: Total heat loss at the satellite frame due to geometry modifications of the insulating washers

Case No.	**Material**				**Total Heat Loss [W]**
	Side Plate	***Bolt***	***Bolt Washer***	***Insulating Washers***	
1	SS	SS	SS	PTFE	**1.6467**
2	SS	SS	SS	PEEK	**1.5923**
3	SS	SS	SS	Polycarbonate	**1.3672**
4	Ti 6Al-4V	SS	SS	Polycarbonate	**1.1915**
5	Ti 6Al-4V	Ti 6Al-4V	Ti 6Al-4V	Polycarbonate	**1.1354**

For reference, the base model dissipated a total heat loss of 2.1604 W at the frame. For all the cases in the table above, the material combination remains the same as in Table 3, with only the geometry modified. For case 1, the total heat loss was reduced by 23.8%. For case 2, the reduction is about 26.3%. For cases 3 through 5, there is a reduction of 36.7%, 44.8% and 47.4%, respectively, in the total heat loss.

3.4.3 Change in Configuration

Another approach to reduce the heat loss at the satellite frame is to change the washer-bolt configuration itself. Since, a majority of the heat from the tank is lost through conduction, the insulating washer that is in direct contact with the tank plays a key role in reducing the heat flow.

By reducing the surface area of contact with the propellant tank, the thermal resistance of the washer-bolt configuration increases significantly, and hence heat loss can be reduced. To achieve a reduced contact area with the tank, a steel serrated washer is placed between the tank and the internal insulating washer. Also, another steel serrated washer is placed between the external insulating washer and the side plate. This configuration is illustrated in Figure 27 and Figure 28.

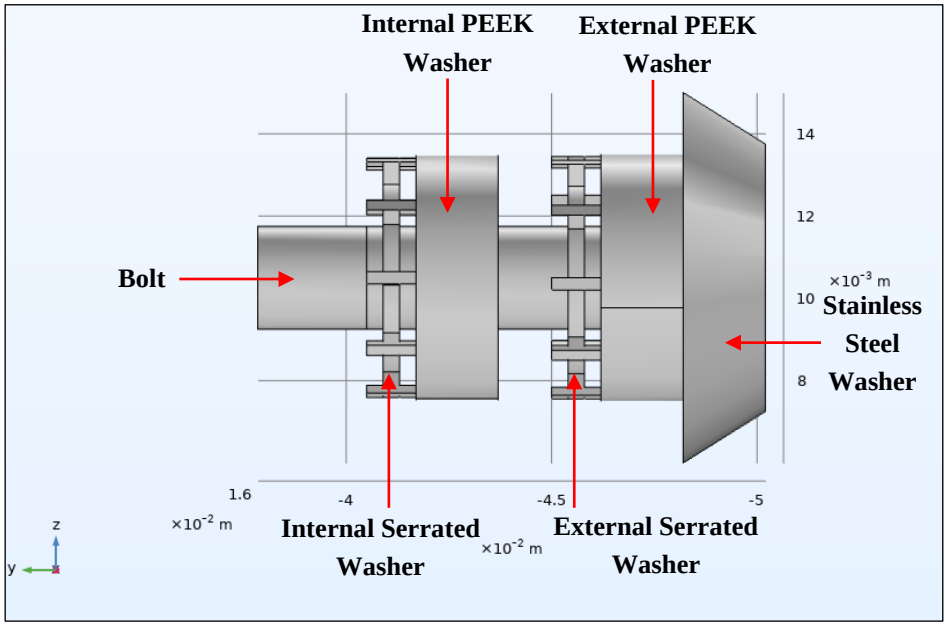

Figure 27: Side view of the bolt-serrated washer configuration

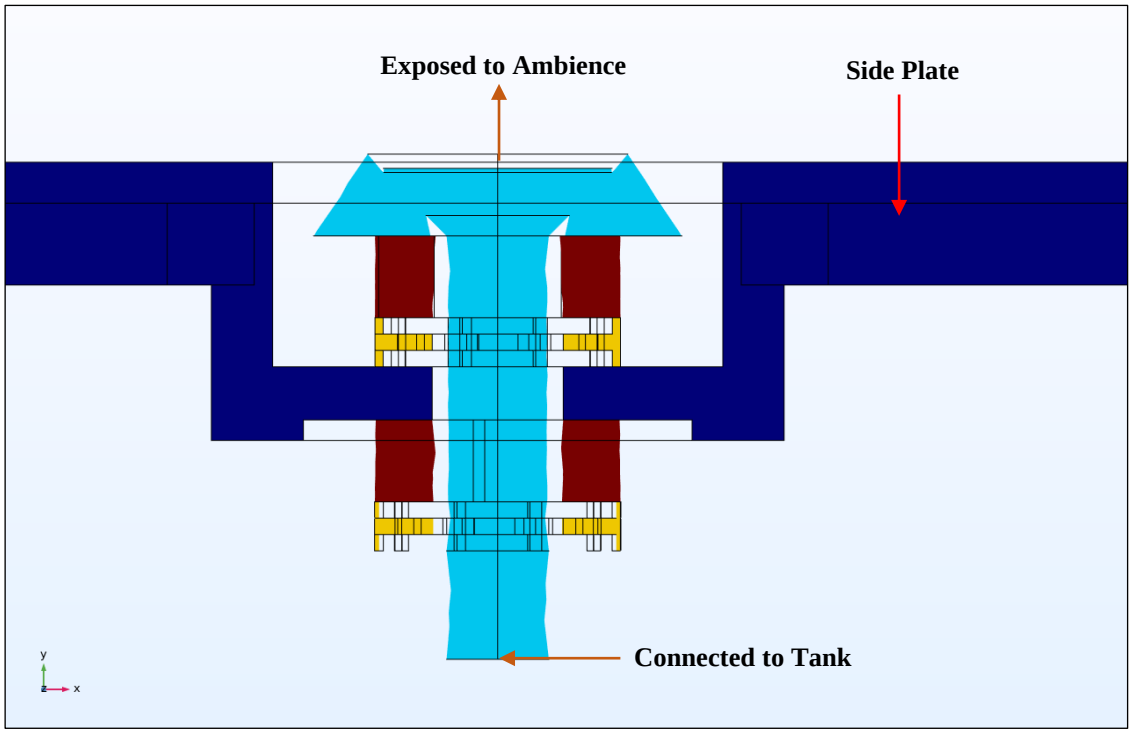

Figure 28: The bolt-serrated washer configuration connected to the I2T5 side plate

A stainless-steel serrated washer was selected as it offered the least surface contact area with the propellant tank. This washer is economic, durable and commercially available.

This new configuration was simulated in COMSOL Multiphysics for conduction heat loss, and the results obtained are tabulated below (Table 5).

Table 5: Total heat loss at the satellite frame for the new configuration

Tank Temperature [°C (K)]	**Satellite Frame Temperature [°C (K)]**	**Heat Loss at the Satellite Frame [W]**
100 (373.15)	-20 (253.15)	0.5686
	0 (273.15)	0.4696
	20 (293.15)	0.3737

Looking at the data in the table above, the heat fluxes obtained for different frame temperatures have reduced significantly. The percentage reductions in heat loss when compared to the base model are: 78.13%, 78.26% and 78.27%. Therefore, an average decrease of 78.2% is observed for the new washer-bolt configuration.

3.4.4 Vacuum Chamber Experiment

3.4.4.1 *Experimental Setup*

The I2T5 was assembled with the new bolt washer configuration (Section 3.4.3), and an experiment was carried out to measure the total heat flux conducted to the satellite frame.

First, the I2T5 thruster was attached to a block of Aluminium 6082-T6 (Figure 29), and was cooled down for several hours. This ensures that the entire system reaches the required steady-state temperature before conducting the experiment. For this study, the initial frame temperature chosen was 0°C, and the data was recorded till around 13°C.

Next, the I2T5 was placed inside a vacuum chamber, which was maintained at room temperature (20°C or 293.15K). The power and the communication cables were connected to the I2T5, as shown in Figure 30, to record the temperatures and power input to the thruster. The tank of the I2T5 was heated to 100°C or 373.15 K.

The motherboard of the I2T5 controls and records the temperature of the tank every second. The frame temperature was measured in 5-minute intervals using a PT-1000 resistor, which gave the resistance in ohms (Ω). This resistance was then translated to temperature values with the help of a standard conversion chart.

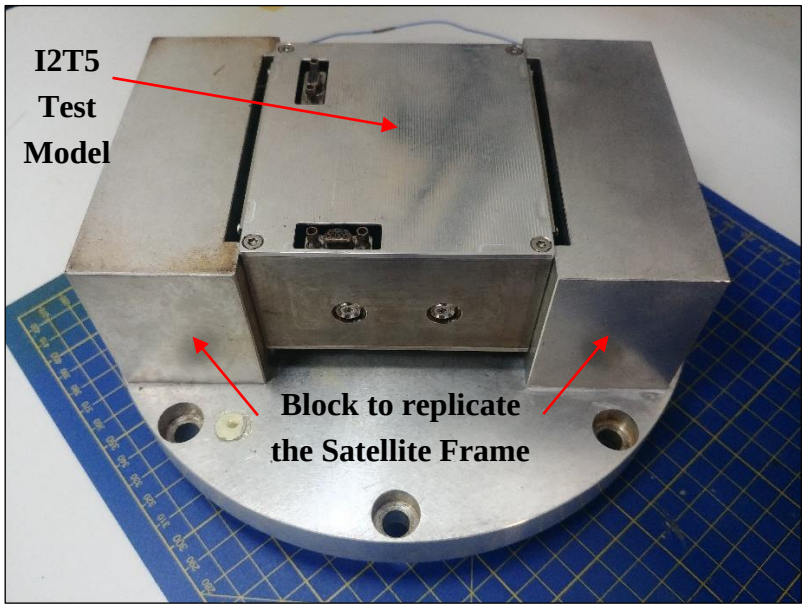

Figure 29: A fully assembled I2T5 thruster fastened to a test block made of aluminium alloy; the block acts as the satellite frame

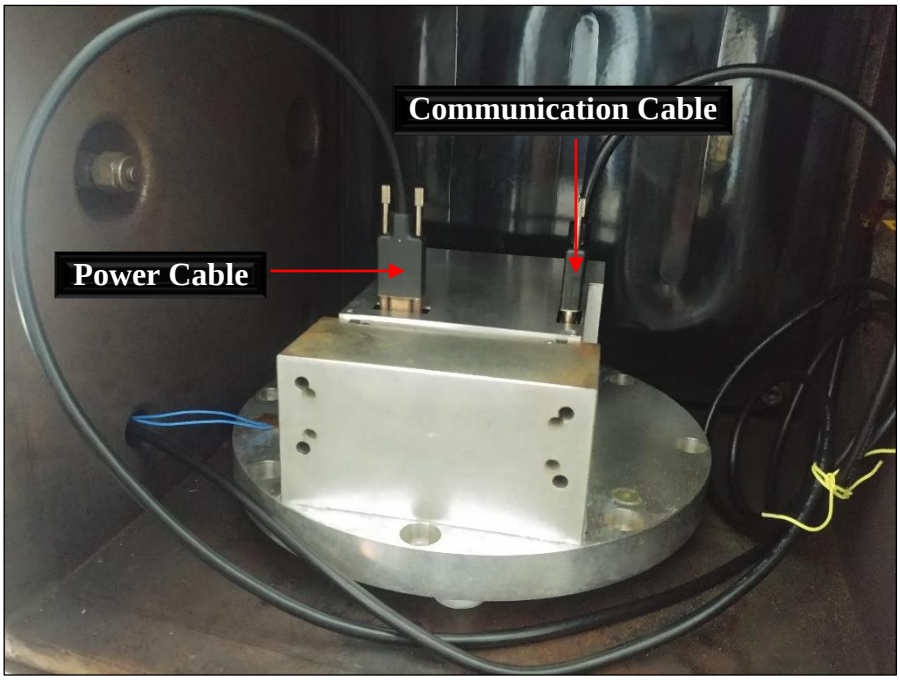

Figure 30: The I2T5 connected and placed inside the vacuum chamber

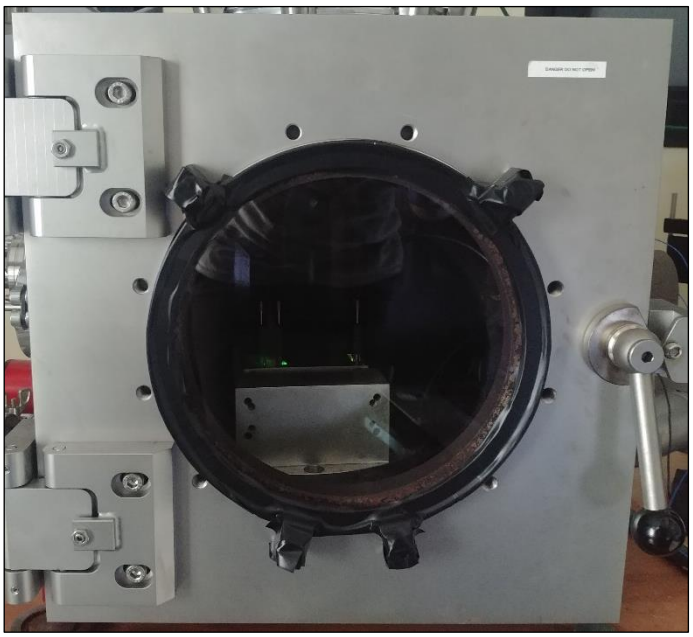

Figure 31: The vacuum chamber used to test the I2T5

The vacuum chamber (Figure 31) uses a primary pump coupled with a turbopump to achieve extremely low pressures. Testing in a vacuum environment is important, as the data recorded would then correlate to the actual flight measurements.

3.4.4.2 *Results*

Using MATLAB, a code was written to post-process the experimental data. The code cleans the data of any outliers, performs curve smoothing, and calculates and plots the total heat loss at the frame.

The formula used to calculate the heat flux at the frame is,

$$\boxed{Q_{frame}[W] = mC_p \frac{dT}{dt}} \tag{15}$$

m → Mass of the Aluminium 6082-T6 block = 3.7 [kg]
C_p → Specific Heat Capacity of Aluminium = 900 $[J/kg.K]$
$\frac{dT}{dt}$ → Rate of change of the block temperature [°C/s or K/s]

Upon plotting the heat flux values, the curve displayed an exponential trend. Hence, the MATLAB curve-fitting toolbox was used to fit an exponential function to the calculated fluxes. The graph obtained is shown in Figure 32.

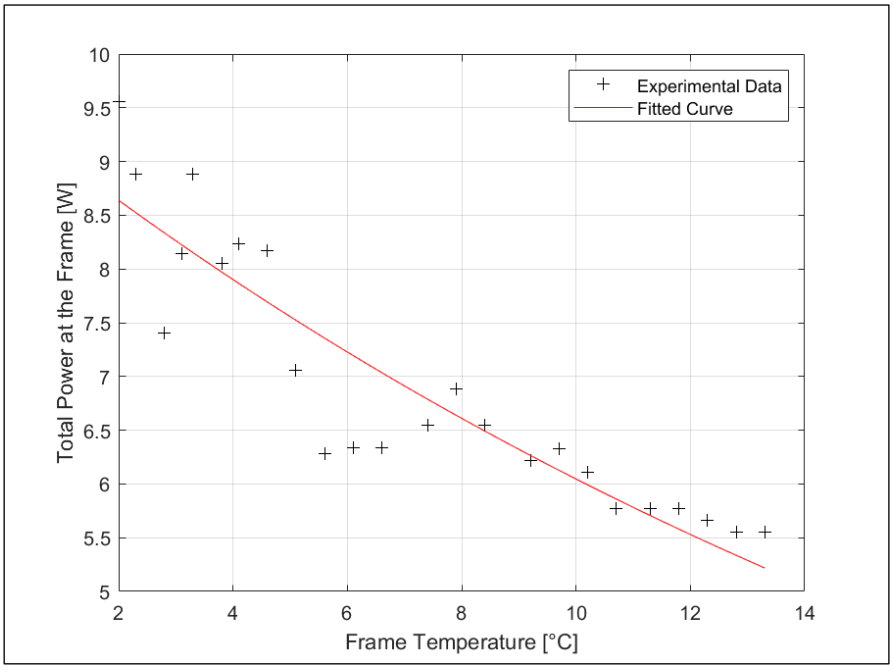

Figure 32: Variation of the total heat loss with the frame temperature for the new configuration

The exponential function obtained from the curve-fitting toolbox was then used to estimate the total heat loss for different frame temperatures (by extrapolation), as shown in Figure 33. This was done to compare the new configuration results with that of the base model.

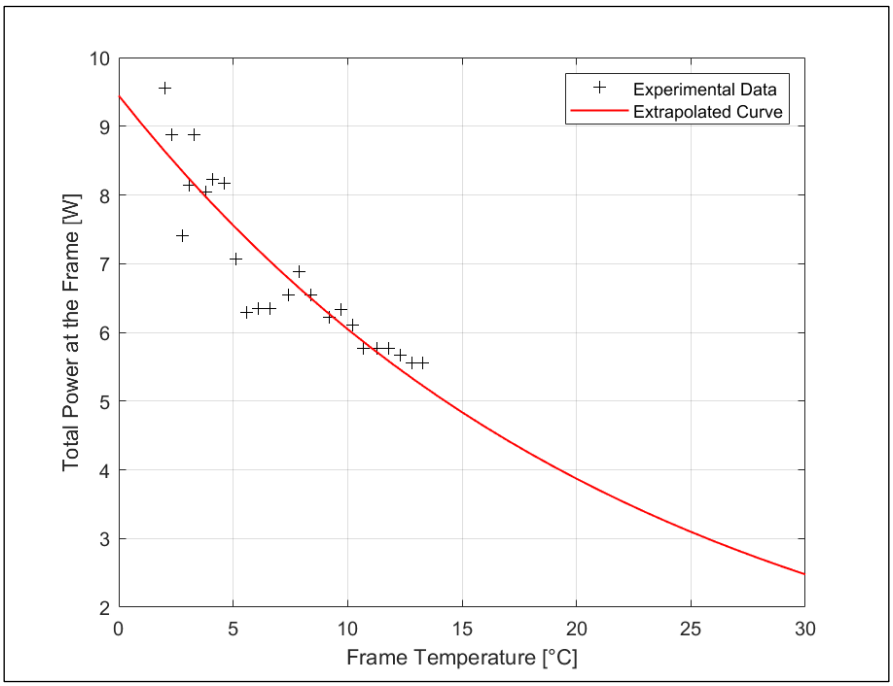

Figure 33: The estimated total heat loss for different frame temperatures for the new configuration

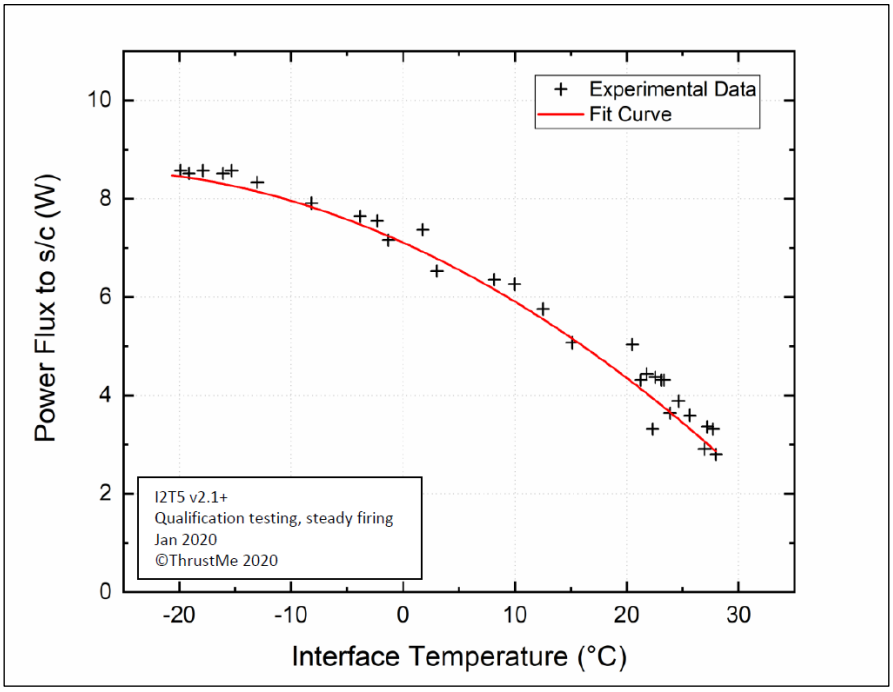

Figure 34: Experimental data corresponding to the base model (Credits: ThrustMe)

Figure 33 shows an extrapolated curve for the new configuration, assuming that the trend will continue as per the fitted function. The concavity of the curve implies that the total heat transferred to the frame decreases with increasing frame temperature, and the rate of change of this curve increases with increasing frame temperature.

Figure 34 shows the fitted curve obtained for the base model. This curve was plotted by the engineers at ThrustMe, and will be used as a reference to verify the results of the new experiment conducted for this thesis work. The concavity of the curve in Figure 34 conveys that the total heat transferred to the frame decreases with increasing frame temperature, and the rate of change of this curve also decreases with increasing frame temperature.

The experimental data points in Figure 32 conveys the existence of perturbations, either external or internal. The potential reasons for these variations could be due to the sudden expansion of the bolts as the temperature rises, and due to the ambient irradiation within the vacuum chamber (as it is at a higher temperature than the frame).

When comparing Figure 33 and Figure 34, the heat fluxes are nearly the same for a frame temperature $> 10°C$, but the total heat loss for the new configuration is slightly less than that of the base model. However, for frame temperature $< 10°C$, the performance of the base model is better than the new configuration.

3.5 Space Thermal Environment Simulation for the I2T5

The next step of the thermal analysis is to determine external heat fluxes of the I2T5, while in space. This section looks at one possible scenario where the I2T5 is attached to a CubeSat orbiting Earth. The results presented here only show the external irradiation that the satellite receives due to the space thermal environment, and does not show the heat flux balance between the internal and external fluxes of the satellite.

To obtain the solar, albedo and Earth IR fluxes for the CubeSat case, the orbital heat flux propagator (or simulator) developed by ThrustMe (refer Appendix – C) was used.

Case Study: A 1-U CubeSat in Sun-Synchronous Orbit

The example scenario described in the conference paper by Posielek, T. [32], was used as a reference to validate the in-house simulator (Appendix – C), and will be used for this case study as well. This paper focuses on developing a Modelica-based library to perform the thermal analysis of a general spacecraft.

The mission parameters for the current study are stated in Table 6. Some of orbital parameters required calculations and assumptions, which have been mentioned.

Table 6: Orbital and CubeSat data for the case study

Parameter	Unit	Value
Type of Orbit	Sun-Synchronous Orbit (SSO)	
Epoch	10 February, 2018 10:00:00	
Semi-major axis, a	km	6977.03 (calculated)
Time period, T	sec	5800
Eccentricity, e	-	0.000864 (calculated)
Inclination, i	deg	98 (assumed for SSO)
RAAN, Ω	deg	180 (= 337.5-157.5; 10:30 h local time)
AOP, ω	deg	0 (assumed)
Mean anomaly, M_e	deg	0
True anomaly, θ	deg	0
Solar constant, G_{sc}	W/m^2	1361
Albedo coefficient		0.3
Absorptivity, α		0.25 (all 6 sides)
Emissivity, ε		0.88 (all 6 sides)
Spacecraft Orientation	Nadir (Earth-pointing)	
Radiative area (s/c face)	m^2	0.01 (all 6 sides)

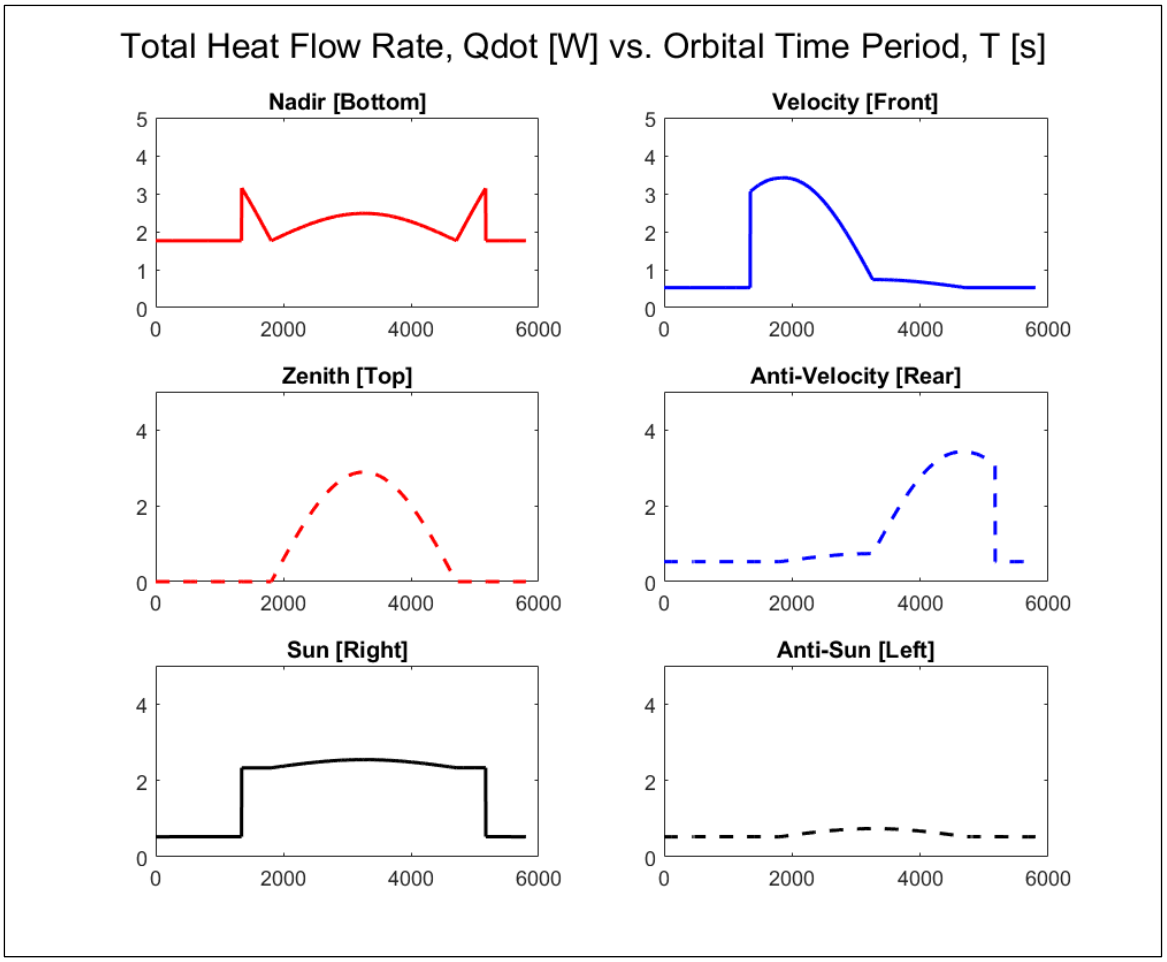

Figure 35: The total heat flux due to solar, albedo and Earth IR irradiation for all six sides of the CubeSat

The satellite presented in [32] has a surface area of 1 m^2 per side of the spacecraft. However, to comply with 1-U CubeSat standards, the area considered for the current study is 0.01 m^2 per surface of the CubeSat.

Figure 35 displays the total heat flux (y-axis) plotted against the orbital time period (x-axis) for each of the six CubeSat surfaces. The graph of interest for this study is the Anti-velocity curve, as it is where the I2T5 thruster could be integrated. The radiation shield of the I2T5 will receive an external flux of 0.5 W (due to Earth IR radiation) for a majority of the orbit, which increases to a maximum value of nearly 4 W, as seen in the plot. The peak in the curve is due to the high intensity of solar flux in the Sun-synchronous orbit during the solar noon [32].

Chapter 4: Discussion

From Table 3 and Table 4, it can be observed that Polycarbonate (PC) is a reasonable substitute for PTFE. Although PEEK is slightly more rigid than PC (refer Appendix – A), the thermal conductivity of the latter is lower. Looking at the side plate material, it is seen that Ti 6Al-4V has a lower thermal conductivity than Stainless Steel. Although, using a Titanium alloy for the side plate reduces the total heat loss compared to Stainless Steel, the minor reduction does not compensate for the high cost of Titanium.

The modification in the geometry of the washers was done by making two semi-circular slots on each washer. By reducing the surface area, the thermal resistance offered by each washer can be increased. Extreme removal of material could compromise the bearing strength of the washer. A possible solution to this integrity problem could be to design the washer such that it possesses a honeycomb structure. This would reduce the overall surface area while maintaining the structural integrity of the washer. This, however, requires a separate study to be conducted, taking the junction mechanical constraints into account.

It can be observed from the new washer-bolt configuration (section 3.4.3) that the serrated washers play a prominent role in minimising conductive heat transfer from the tank to the satellite frame. From the vacuum chamber experimental results, it is evident that there are other sources of heat loss present, mainly internal radiation, and external radiation. However, more experiments need to be conducted to quantify the other losses.

The mechanical coupling of the PEEK insulating washers and serrated washers could result in an undesirable situation during rocket launch (high G-force) wherein, the serrated washers could pierce the PEEK washers. Hence, extensive vibrational testing has to be conducted to ensure the stability of this combination of washers. A possible solution to this coupling problem is to place a thin metal washer (either steel or aluminium alloy) at the interface between the PEEK and serrated washers.

For the experimental data obtained (section 3.4.4.2), the total heat loss constitutes radiation, conduction and physical (due to material defects) losses. Hence, the data can only be compared to the experiment that was performed for the base model. The simulation results in section 3.4.3 only shed light on the conductive heat losses due to the washer-bolt configuration, and only forms a part of the total heat loss (experimental value) at the frame.

Chapter 5: Conclusion

The conductive heat loss issue of the I2T5 thruster was addressed by running thermal simulations in COMSOL Multiphysics. The key factor of the solution was found to be in the thermal contact between the propellant tank and the insulating washers of the washer-bolt configuration, which fastens the side plate of the I2T5 to the tank. Here, the washer-bolt configuration refers to the bolts, bolt washers and insulating washers.

The study is first conducted for a combination of different insulating washer materials, followed by a modification of the insulating washer geometry. When only considering a change in material of the base model, the combination of stainless-steel for the side plate, bolt and bolt washer, and polycarbonate for the insulating washers seems to be the most feasible option, as it resulted in a total heat loss reduction of 35.6%. A combination of changing the materials and also modifying the geometry resulted in a 47.4% total heat loss reduction when compared to the base model.

Although the heat loss was reduced by nearly 50%, there was still scope for improvement. A new study was considered, wherein, two stainless-steel serrated washers were introduced in the washer-bolt configuration. Due to the minimal surface contact area between the serrated washer and the propellant tank, the total heat flux was reduced by 78.2% which looks to be promising.

All the thermal simulations were successful in decreasing the total heat lost to the satellite frame due to conduction only, but it was necessary to test the new washer-bolt configuration experimentally. For this purpose, a test model of the I2T5 was attached to an aluminium block which acted as the satellite frame. The I2T5 was then tested in a vacuum chamber at room temperature or 20°C (293.15 K). The variation of the total heat loss obtained for different satellite frame temperatures was observed to be: (1) more than the base model for frame temperature $< 10°C$, and (2) less than the base model for frame temperature $> 10°C$. This variation can be attributed to errors in measurements, or the curve fitting function used. The experiment can be repeated, but starting at a lower frame temperature (for e.g., -20°C), so that the entire system has sufficient time to stabilise. Furthermore, additional experiments have to be conducted to identify all other sources of heat loss, besides conduction.

The new washer-bolt configuration requires physical testing to confirm that the thermal resistance between the propellant tank and satellite frame has increased, as seen in the respective simulation. Thus, the total heat loss problem of the I2T5, due to conductive heat transfer only, has been alleviated as verified by the thermal simulations, but extensive experimentation is recommended to determine the actual performance.

Chapter 6: Future Work

6.1 Thermal Simulations

There are many interesting materials that could insulate the heat flow from the tank effectively. Kevlar is one such material, as it has a very low thermal conductivity (around $0.04\ W/m.K$). However, as it is a fabric, it has to be coated with an epoxy resin to bolster its compressive strength. As a consequence, this would increase the thermal conductivity of the Kevlar-resin composite.

All the simulations focused on the conductive heat flux from the tank to the satellite frame. Hence, a study involving radiative heat transfer should also be performed to ensure a thorough analysis of the I2T5.

The study in section 3.5 can be extended to test the thermal capability of the I2T5 while in orbit. A transient analysis has to be conducted for the same, which should also include the heat transfer due to radiation. Furthermore, the performance of the I2T5 can be tested for different orbits and CubeSat configurations.

6.2 Experimentation

Due to time constraints and limited access to the vacuum chamber, the I2T5 could only be tested once for the new configuration. Therefore, there is scope for additional testing at lower frame temperatures (around -20°C).

The I2T5 can also be tested for different washer-bolt configurations, and this can be compared to the simulations, provided that the experimental block (makeshift satellite frame) is modelled, and radiative heat transfer is included in the analysis.

Chapter 7: References

[1] S. Loff, "CubeSats Overview," *www.nasa.gov*, 2018. https://www.nasa.gov/mission_pages/cubesats/overview (accessed Jul. 22, 2020).

[2] M. Swartwout, "The first one hundred CubeSats : A statistical look," *J. Small Satell.*, vol. 2, no. 2, pp. 213–233, 2013.

[3] E. Kulu, "Nanosats Database." www.nanosats.eu (accessed Jul. 28, 2020).

[4] H. Curtis, "CubeSat thrusters: an overview of in-space propulsion products for small satellites," 2019. https://blog.satsearch.co/2019-07-10-cubesat-thrusters-an-overview-of-in-space-propulsion-products-for-small-satellites (accessed Jul. 20, 2020).

[5] A. C. Tribble, *The Space Environment: Implications for Spacecraft Design*, vol. 17, no. 4. Princeton University Press, Princeton, NJ, 1997.

[6] K. Lemmer, "Propulsion for CubeSats," *Acta Astronaut.*, vol. 134, no. January, pp. 231–243, 2017, doi: 10.1016/j.actaastro.2017.01.048.

[7] G. Sutton and O. Biblarz, *Rocket Propulsion Elements*, Ninth. John Wiley & Sons, 2016.

[8] J. M. Martínez, D. Rafalskyi, E. Z. Rossi, and A. Aanesland, "Development, Qualification and First Flight Data of the Iodine Based Cold Gas Thruster for CubeSats," in *IAA Conference on University Satellite Missions and CubeSat*, 2020, p. 15, doi: 10.6084/m9.figshare.11931384.

[9] T. L. Bergman, F. P. Incropera, D. P. DeWitt, and A. S. Lavine, *Fundamentals of Heat and Mass Transfer*, Seventh. John Wiley & Sons, 2011.

[10] M. Thirumaleshwar, *Fundamentals of Heat and Mass Transfer*. Pearson Education, India, 2006.

[11] E. A. Silk, *Introduction to Spacecraft Thermal Design*. Cambridge University Press, 2020.

[12] J. Meseguer, I. Pérez-Grande, and A. Sanz-Andrés., *Spacecraft Thermal Control*. Elsevier, 2012.

[13] D. G. Gilmore, *Spacecraft Thermal Control Handbook Volume I : Fundamental*

Technologies, Second., vol. I. El Segundo, CA: The Aerospace Press, 2002.

[14] R. D. Karam, *Satellite Thermal Control for Systems Engineers*. American Institute of Aeronautics and Astronautics, 1998.

[15] A. B. Uygur, "A Complete Methodology for the Computation of External Heat Fluxes for the Transient Thermal Analysis of Satellites," *J. Aeronaut. Sp. Technol.*, vol. 11, no. 1, pp. 17–27, 2018.

[16] W. J. Larson and J. R. Wertz, *Space Mission Analysis and Design*, Third. Microcosm Inc., 2005.

[17] R. N. Miyake, "Spacecraft Design Thermal Control Subsystem," Pasadena, CA, USA, 2008. [Online]. Available: https://trs.jpl.nasa.gov/handle/2014/41701.

[18] L. Klintberg, M. Karlsson, L. Stenmark, J. Å. Schweitz, and G. Thornell, "A Large Stroke, High Force Paraffin Phase Transition Actuator," *Sensors Actuators A Phys.*, vol. 96, no. 2–3, pp. 189–195, 2002.

[19] H. J. Kramer, "TacSat-4 - Satellite Missions," 2002. https://earth.esa.int/web/eoportal/satellite-missions/t/tacsat-4#GVMwF12eHerb (accessed Aug. 03, 2020).

[20] P. M. Dussinger, D. B. Sarraf, and W. G. Anderson, "Loop Heat Pipe for TacSat-4," in *AIP Conference Proceedings*, 2009, p. Vol. 1103, No. 1, pp. 91–100.

[21] I. Garmendia, E. Anglada, H. Vallejo, and M. Seco, "Accurate calculation of conductive conductances in complex geometries for spacecrafts thermal models," *Adv. Sp. Res.*, vol. 57, no. 4, pp. 1087–1097, Feb. 2016, doi: 10.1016/j.asr.2015.12.027.

[22] E. C. S. S. Secretariat, *Thermal Design Handbook-Part 4: Conductive Heat Transfer*. Noordwijk, The Netherlands: ESA-ESTEC, 2011.

[23] J. S. Lewis, *Physics and Chemistry of the Solar System*, Second. Tucson, Arizona: Academic Press, 2004.

[24] E. A. Thornton, *Thermal Structures for Aerospace Applications*. American Institute of Aeronautics and Astronautics, 1996.

[25] D. Salvi, D. Boldor, J. Ortego, G. M. Aita, and C. M. Sabliov, "Numerical Modeling of Continuous Flow Microwave Heating: A Critical Comparison of COMSOL and

ANSYS," *J. Microw. Power Electromagn. Energy*, vol. 44, no. 4, pp. 187–197, 2010.

[26] M. Vajdi, F. Sadegh Moghanlou, F. Sharifianjazi, M. Shahedi Asl, and M. Shokouhimehr, "A Review on the Comsol Multiphysics Studies of Heat Transfer in Advanced Ceramics," *J. Compos. Compd.*, vol. 2, no. 1, pp. 35–44, Feb. 2020, doi: 10.29252/jcc.2.1.5.

[27] I. Martínez, "Radiative View Factors," *Universidad Politécnica de Madrid*. http://webserver.dmt.upm.es/~isidoro/tc3/Radiation View factors.pdf (accessed Jun. 20, 2020).

[28] D. J. Fixsen, "The Temperature of the Cosmic Microwave Background," *Astrophys. J.*, vol. 707, no. 2, p. 916, 2009, [Online]. Available: https://iopscience.iop.org/article/10.1088/0004-637X/707/2/916/meta.

[29] J. Scialdone, P. Isaac, C. Clatterbuck, and R. Hunkeler, "Material Total Mass Loss in Vacuum Obtained from Various Outgassing Systems," 2000. [Online]. Available: https://ntrs.nasa.gov/search.jsp?R=20010038656.

[30] A. Fisher and B. Mermelstein, "A Compilation of Low Outgassing Polymeric Materials Normally Recommended for GSFC Cognizant Spacecraft," NASA TM X-65705, 1971.

[31] N. A. Walter and J. J. Scialdone, "Outgassing Data for Selecting Spacecraft Materials," NASA, 1997.

[32] T. Posielek, "A Modelica Library for Spacecraft Thermal Analysis," 2018, doi: 10.3384/ECP1815445.

[33] D. A. Vallado, *Fundamentals of Astrodynamics and Applications*, First. McGraw-Hill Primis Custom Publishing, 1997.

[34] H. D. Curtis, *Orbital Mechanics for Engineering Students*, Fourth. Butterworth-Heinemann, 2020.

[35] Y. Shabany, "Component Size and Effective Thermal Conductivity of Printed Circuit Boards," in *ITherm 2002. Eighth Intersociety Conference on Thermal and Thermomechanical Phenomena in Electronic Systems (Cat. No.02CH37258)*, 2002, pp. 489–494, doi: 10.1109/ITHERM.2002.1012496.

Chapter 8: Appendices

8.1 Appendix – A

Material Properties

Mechanical properties like strength, toughness, rigidity, hardness and fatigue are required to ensure that the component can sustain extreme G-forces and vibrations. Thermal properties like thermal conductivity and specific heat capacity are important for a thermal conduction study.

Table 7 presents a list of materials that were chosen for the study based on their thermal and mechanical properties. COMSOL requires density, thermal conductivity and specific heat capacity as input for all conductive heat transfer studies. Young's modulus determines the rigidity of a material, and as the insulating washers of the washer-bolt are compressed, they need to possess good rigidity and bearing strength.

Table 7: Mechanical and thermal properties of materials used for the study (Credits: SPACEMATDB; AZoM; MatWeb material database)

Material	Properties			
	Young's Modulus (GPa)	**Density (kg/m^3)**	**Thermal Conductivity (W/m-K)**	**Specific Heat Capacity (J/kg-K)**
Insulating Washers				
Teflon (PTFE)	0.6	2200	0.25	1000
Tecapeek (PEEK)	3.6	1320	0.24	1340
Makrolon-6555 (Polycarbonate)	2.4	1200	0.20	1200
Side Plate				
Stainless Steel (SS)	200	7850	16	475
Ti 6Al-4V (Titanium Alloy)	113.8	4430	6.7	526.3

8.2 Appendix – B

Validation of the View Factors Derived by COMSOL

COMSOL Multiphysics derives and computes the radiative view factors when surface-to-surface radiation is in effect. This section looks at comparing the view factor value obtained from COMSOL to that obtained analytically. The errors are tabulated in Table 8.

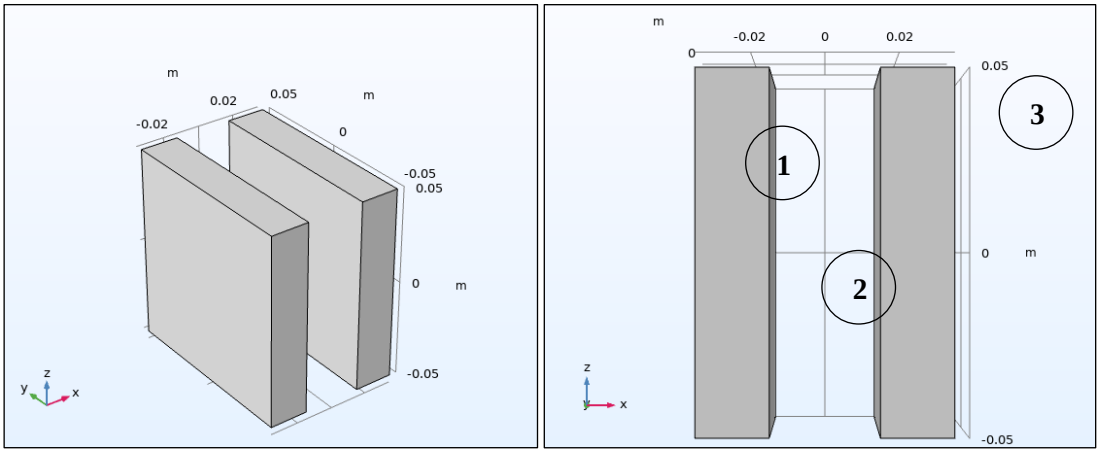

Figure 36: Two identical and parallel square plates designed in COMSOL; isometric view (left) and side view (right)

Consider the two $10 \times 10 \times 2$ cm plates separated by a distance of 3 cm, shown in Figure 36. Assume that the radiative heat transfer is between surface (1) and surface (2) shown in the side view. Since the system is open, the two surfaces also radiate heat to the ambient (3), which is considered to be a blackbody absorbing all the incoming radiation. Since the ambient is large, the fraction of radiation from the ambient to the two surfaces can be assumed to be zero. This implies that $F_{31} = F_{32} = 0$ and hence, $F_{33} = 1$. As the two surfaces are flat, radiation emitted by either surface does not fall back on itself, hence $F_{11} = F_{22} = 0$. Surfaces (1) and (2) have equal area, hence from the relation, $A_1F_{12} = A_2F_{21}$, it can be deduced that $F_{12} = F_{21}$. Finally, from the view factor summation rule, i.e., $\sum_{j=1}^{N} F_{ij} = 1$, the surface-to-ambient radiation is, $F_{13} = 1 - F_{11} - F_{12}$ and by symmetry, $F_{23} = F_{13}$.

A comprehensive list of view factors for various geometries can be found in [27]. For two identical, parallel square surfaces of side W, separated by a distance, H, with $w = \frac{W}{H}$, the view factor is given by [27],

$$\boxed{F_{12} = \frac{1}{\pi w^2}\left(\ln\left(\frac{x^4}{1+2w^2}\right) + 4wy\right)} \tag{16}$$

Where, $x = \sqrt{1+w^2}$ and $y = x\tan^{-1}\left(\frac{w}{x}\right) - \tan^{-1} w$

Table 8: A comparison of the view factors obtained through the numerical and analytical methods, with the respective computational errors

View Factor (F_{ij})	**Numerical Value (COMSOL)**	**Analytical Value (Formula)**	**Error (*Numerical – Analytical*)**
F_{11}	0	0	0
F_{12}	0.57953	0.57953	4.8409×10^{-6}
F_{13}	0.42047	0.42047	4.8409×10^{-6}
F_{21}	0.57953	0.57953	3.8142×10^{-6}
F_{22}	0	0	0
F_{23}	0.42047	0.42047	3.8142×10^{-6}
F_{31}	0	0	0
F_{32}	0	0	0
F_{33}	1	1	0

As observed in Table 8, the view factors derived by COMSOL Multiphysics are adequately accurate to be used for the radiation analysis. Note that, using a finer mesh for the models can result in more accurate solutions, at the cost of large computation times.

8.3 Appendix – C

The ThrustMe Propagator for the In-Orbit Thermal Characterisation of a Spacecraft

This orbital propagator is designed and developed by Javier Martínez Martínez, Lead R&D Fluidics Engineer, ThrustMe. It is applicable to the thermal characterization (i.e., evaluation of the orbital environment heat fluxes) of a CubeSat of any form factor. This program takes into account the J2 perturbations (due to the oblateness of Earth), as well as the ecliptic effects on a satellite moving in the shadow of Earth. As a subsidiary part of this thesis, the formulae used for the propagator were cross-verified by referring to the books authored by E.A. Thornton, D.A. Vallado and H.D. Curtis [24], [33], [34]. Table 9 below summarizes the input and output pertaining to the code.

Table 9: Input and output parameters for the heat flux simulator

Input	**Output**
• Keplerian orbital parameters [a, e, i, Ω, ω *and* M_e] • Epoch (*Gregorian/Julian*) • Average solar flux [W/m^2] • Albedo factor • Surface Emissivity, ε and Absorptivity, α of each face • Spacecraft orientation (*Nadir/Sun*) • Number of orbits • Surface area of each face [m^2]	• Solar flux [W *or* W/m^2] • Earth Infrared flux [W *or* W/m^2] • Albedo flux [W *or* W/m^2] • Total heat flux [W *or* W/m^2] • Keplerian orbital parameters at the end of propagation

a → Semi-major axis e → Eccentricity i → Inclination	Ω → Right-Ascension of the Ascending Node (RAAN) ω → Argument of Periapsis (AOP) M_e → Mean anomaly

8.4 Appendix – D

Thermal Conductivity of the I2T5 Motherboard

A Printed Circuit Board (PCB) is made of multi-layered FR4 (a glass-reinforced epoxy laminate) with embedded copper wiring. As a result of this combination, the thermal conductivity of the PCB is anisotropic [35]. Therefore, it is generally modelled as a single component with parallel (across the board surface) and normal (across the board thickness) effective thermal conductivities, and the heat conduction is assumed as one-dimensional, and without any contact resistance between layers.

For a PCB with thickness, t, having N_g number of glass-epoxy layers, and N_c number of copper layers, the effective parallel and normal thermal conductivities, k_{par_e} and k_{nor_e}, respectively are given by [35],

$$k_{par_e} = \frac{\sum_{i=1}^{N_g} k_g t_{g_i} + \sum_{i=1}^{N_c} k_c t_{c_i}}{t} \tag{17}$$

$$k_{nor_e} = \frac{t}{\sum_{i=1}^{N_g} {t_{g_i}}/{k_g} + \sum_{i=1}^{N_c} {t_{c_i}}/{k_c}} \tag{18}$$

k_g → Thermal conductivity of glass-epoxy $[W/m.K]$
k_c → Thermal conductivity of copper $[W/m.K]$
t_{g_i} → Thickness of the i^{th} glass-epoxy layer $[m]$
t_{c_i} → Thickness of the i^{th} copper layer $[m]$

Using equations (17) and (18), for $k_g = 0.3\ W/m.K$, and $k_c = 390\ W/m.K$, the effective parallel and normal thermal conductivities for the I2T5 motherboard were found to be, $k_{par_e} = 31.165\ W/m.K$, and $k_{nor_e} = 0.325\ W/m.K$, for a board thickness, $t = 1.553\ mm$.